Possible (closed system) pingo and ice-wedge/thermokarst complexes at the mid latitudes of Utopia Planitia, Mars

R.J. Soare, Susan J. Conway, J.-P. Williams, C. Gallagher, L.E. Mc Keown

12/03/2019 8:13 PM

Possible (closed system) pingo and ice-wedge/thermokarst complexes at the mid latitudes of Utopia Planitia, Mars

R.J. Soare,[1] S.J. Conway,[2] J-P Williams,[3] C. Gallagher,[4] and L.E. Mc Keown[5]

[1]Geography Department, Dawson College,
Montreal, QC, H3Z 1A4, Canada
(rsoare@dawsoncollege.qc.ca)

[2]CNRS UMR 6112, LPG, Nantes, France

[3]Department. of Earth, Planetary and Space Sciences,
University of California, Los Angeles, CA, 90095, USA

[4]School of Geography, University College Dublin, Belfield, Dublin 4, Ireland

[5]Geography Department, Trinity College Dublin, Dublin 2, Ireland

Pages: 45

Figures: 11

Tables: 1

Keywords: Mars surface, climate, ices

Abstract

On Earth, hydrostatic or closed-system pingos (*CSPs*) are perennial ice-cored mounds formed by the freeze-thaw cycling of water when or as thermokarst lakes lose their water by drainage or evaporation. The mounds vary in shape from circular or sub-circular to elongate, are sub-kilometre in their long axes, and may reach decametres in height. Often, the mounds show summit depressions, radial fractures and single tiers or benches. As the *CSPs* degrade, small-scale debris flows or slumps occur; end-stage degradation typically exhibits debris-laden ramparts elevated metres above the surrounding terrain.

Typically, the *CSPs* originate and develop where deep and continuous permafrost is ice-rich, i.e. infused with excess ice, as it is in the Tuktoyaktuk Coastlands of northern Canada, mid to northern Alaska and northeast Russia. In these areas or regions the terrain often is populated by: **a)** thermokarst lakes and alases (thermokarst lake basins absent of water); **b)** fields of small-scale ice-wedge polygons (either low-centred or high-centred relative to the polygon margins); and, **c)** melt-water filled or emptied polygon-margin troughs or -corner pits. Individual troughs and pits connected by means of the local topographical gradient comprises beaded stream systems or networks.

Here, we report, describe and discuss a suite of candidate *CSPs* at the mid-latitudes of Utopia Planitia (*UP*) (~35-50^{o} N; ~80-115^{o} E). The morphologies, scale and height of the Martian mounds, as well as the surface textures and characteristics, landscape features and spatially-associated landforms, are consistent with the *CSPs* observed in ice-rich regions on Earth.

The *UP* mounds are nested in or reside adjacent to: flat-floored, possibly thermokarstic depressions; small-scale polygons (some of which exhibit low or high centres relative to their margins); and, connected polygon-margin depressions or pits that mirror beaded-stream systems

in ice-rich terrain on Earth. The size-frequency distribution of craters in our study region precludes a surface younger than ~100 Ma. Thus, the *CSP*-like mounds in *UP* and the pre-mound periglacial-revisions of the landscape presented by us may be markers of freeze-thaw cycling that occurred much earlier in the Amazonian Epoch than most of the current discussions about periglaciation in *UP* suggest.

Introduction

Here, we report, describe and evaluate the presence, distribution and possible origin of sub-kilometre, circular or sub-circular mounds at the mid-latitudes of Utopia Planitia (*UP*) (~35-50^{o} N; ~80-100^{o} E) **(Fig. 1)**. The mounds are observed in the midst of or adjacent to relatively flat-floored and rimless depressions that may or may not be scalloped, are metres to decametres deep and, where they show spatial intersection, are kilometres in reach. Typically, the terrain within and without the depressions is polygonised. Metres-deep polygon-margin troughs or corner pits are extensive, often connected, and follow the local/regional topographical gradient, i.e. south-north. Some of the mounds exhibit metres-wide (mound-diameter) cracks; some of these cracks intercept polygon margins in the surrounding terrain.

Mounds on Earth that show similarities of shape, scale, height, surface characteristics, landscape features, and spatially-associated landforms, occur in regions of ice-rich and deep continuous permafrost. The mounds are closed-system (hydrostatic) pingos (*CSPs*), i.e. perennial mounds that are ice-cored and formed from the freeze-thaw cycling of near-surface water (e.g. Mackay, 1998). We propose that the candidate Martian *CSPs* are rooted in a cold-climate (albeit paleo-) hydrological system, akin to ice-rich periglacial landscapes on Earth where liquid water exhibits seasonal stability.

Speculation concerning the existence of Martian pingos dates back to the Mariner and Viking missions of the 1960s and 1970s and carries through to the present day (e.g. Anderson et al., 1967, Lucchitta, 1981; Rossbacher and Judson, 1981; Parker et al., 1993; Burr et al., 2005; Soare et al., 2005; de Pablo and Komatsu, 2009; Dundas et al., 2008; Dundas and McEwen, 2010; Soare et al., 2013, 2014b). The hypothesised connexion between pingo-like mounds on Mars and ice-rich terrain is no less apparent through the deep history of Mars' remote-exploration (e.g. Anderson et al., 1967, Lucchitta, 1981; Rossbacher and Judson, 1981; Costard and Kargel, 1995; Soare et al., 2005, 2013).

Below, we: **1)** describe and discuss the candidate *CSPs* in *UP*, as well the local landscapes and features that are relevant to the sustenance of our pingo hypothesis; **2)** present the key geological elements of periglacial landscapes on Earth where *CSPs* are commonplace; and, **3)** develop a landscape-scale geochronology of pingo origin and growth that is derived of possible landscape analogues on Earth but consistent with recent work on the Late Amazonian Epoch evolution of Mars.

2. Methods

This study surveys all of the available High Resolution Imaging Science Experiment (*HiRISE*), Mars Reconnaissance Orbiter (*MRO*) (McEwen et al., 2007) images within our study region (N=513). The data-base of *HiRISE* sites (n=9) and images (n=12) relevant to our *CSP* hypothesis is presented in **Table 1**. Images produced by the Mars Odyssey's Thermal Emission Imaging System (*THEMIS*) (Christensen et al., 2004) and the *MRO*'s Context Camera (*CTX)* Malin et al., 2007) provide a regional context.

Using the Cratertools plug-in for the *ESRI ArcGIS* (Kneissl et al., 2011) to measure crater diameters, crater counts were conducted to characterize the surface ages and modification rates of

the terrain incised by the rimless and sometimes scalloped depressions and populated by the pingo-like mounds relative to crater production. Crater size-frequency distributions (*CSFDs)* were compared with crater production functions and model ages using Craterstats (Michael and Neukum, 2010) and the crater-chronology system of Hartmann (2005).

3. Observations: pingo-like mounds and a possible "wet" periglacial landscape in Utopia Planitia

Amidst rimless, irregularly-shaped depressions that may show scalloped morphologies, small-sized (~≤100 m in diameter) circular or sub-circular mounds (metres to decametres in elevation) **(Figs. 2a-f)** are observed at the mid-latitudes of Utopia Planitia **(Fig. 1); Table 1)**. Some of the mounds are domed **(Figs. 2e-f)**; some of them feature summit depressions **(Figs. 2b; 3a-b)**, of varying surface areas and depths **(Figs. 2b; 3a-b)**; and, some of them have centres almost completely depleted of mass and elevation (above the surrounding terrain, leaving only metre-scale raised rims in their wake **(Fig. 3b-c)**. Often, the mounds host decametres-long and metres-wide radial cracks **(Fig. 2f)**. In turn, some of these cracks intercept polygon margins in the surrounding terrain **(Figs. 2e-f)**.

The rimless depressions are metres to decametres deep (e.g. Morgenstern et al., 2007; Lefort et al., 2009; Séjourné et al., 2011) and exhibit long axes that are decametres to hundreds of metres in reach **(Figs. 4a-b, d)**. They may be singular, dense or clustered in their distribution **(Figs. 4a-b, d)** and the collective reach of the depressions, where they overlap, often is kilometres in scale (e.g. Seibert and Kargel, 2001; Morgenstern et al., 2007; Soare et al., 2008; Lefort et al., 2009; Ulrich et al., 2010; Séjourné et al., 2011) **(Figs. 4a-b, d)**.

Inward-oriented scarps (relative to the depression floors) may occur within the larger depressions **(Fig. 4b)**; they comprise incremental losses of elevation that range from metres to

120 decametres (e.g. Morgenstern et al., 2007; Soare et al., 2008; Lefort et al., 2009; Séjourné et al.,
121 2011). The majority of scarps exhibit a poleward orientation and form on the southern margin of
122 the depressions (e.g. Morgenstern et al., 2007; Lefort et al., 2009; Ulrich et al., 2010; Séjourné
123 etal., 2011). A minority of scarps exhibit an equatorward orientation and form on the northern
124 margin of the depressions (e.g. Morgenstern et al., 2007; Lefort et al., 2009; Ulrich et al., 2010;
125 Séjourné et al., 2011). Some depressions exhibit no scarps **(Fig. 4d)**. The number of scarps seems
126 to be relative to the surface area and depth of the depressions, i.e. expansive and deep depressions
127 often show multiple scarps whereas small and shallow depressions typically are absent of scarps
128 (Lefort et al., 2009; Ulrich et al., 2010).

129 Typically, the depressions are incised by small-sized (metre to decametre-scale) polygons
130 (e.g. Morgenstern et al., 2007; Soare et al., 2008; Lefort et al., 2009; Séjourné et al., 2011) (**Fig.**
131 **4c)**. The polygonised terrain also is observed outside of or without the depressions **(Figs. 4a-c)**.
132 Here, the polygons are slightly larger than those observed within the depressions (Morgenstern et
133 al., 2007; Lefort et al, 2009; Ulrich et al., 2010; Séjourné et al., 2011). Some polygons exhibit
134 raised margins or shoulders, relative to their centres (*LCPs*) **(Fig. 4e)**; others show depressed
135 margins, relative to their centres (*HCPs*) **(Fig. 4e)** (Ulrich et al. 2010; Séjourné et al., 2011; Soare
136 et al., 2018d).

137 Some polygon-margins exhibit fissures that are linear or sub-linear, metres wide and deep
138 **(Fig. 4c)** (e.g. Wan Bun Tseung and Soare, 2006; Morgenstern et al., 2007; Lefort et al., 2009;
139 Ulrich et al., 2010; Séjourné et al., 2011; Soare et al., 2011). Polygon-margin junctions may
140 comprise irregular circular to sub-circular pits whose minor axes are slightly wider than the
141 fissures or pits exhibited by the linear or sub-linear margins fissures **(Fig. 4c)** (e.g. Wan Bun
142 Tseung and Soare, 2006; Morgenstern et al., 2007; Lefort et al., 2009; Ulrich et al., 2010; Séjourné

et al., 2011; Soare et al., 2011). Some of the fissures or pits are linked spatially and trend along their north-south axes **(Fig. 4e)** (Wan Bun Tseung and Soare, 2006; Morgenstern et al., 2007; Lefort et al., 2009; Séjourné et al., 2010; Ulrich et al., 2010; Séjourné et al., 2011; Soare et al., 2011).

4. Closed-system pingos, and ice-(rich) complexes on Earth

4.1 Closed system pingos

In regions such as the Tuktoyaktuk Coastlands (*TC*) of northern Canada (e.g. Porsild, 1938; Müller, 1962; Rampton, 1988; Mackay, 1998, 1999; Samsonov et al., 2016), mid- to northern Alaska (e.g. Leffingwell, 1915; Porsild, 1938; Cabot, 1947; Hinkel et al., 2005; Wetterich et al., 2012) and northeast Russia (e.g. Schirrmeister et al., 2002, 2018; Morgenstern et al., 2013; Vasil'chuk et al., 2016; Wetterich et al. 2018), mounds that show similarities of scale, shape, morphological characteristics and landscape features to the Martian *CSP*-like mounds dot the landscape **(Fig. 2e)**. These mounds - hydrostatic or closed-system pingos (*CSPs*) - exhibit perennial ice-cores.

Typically, the *CSPs* originate on the floors of thermokarst lakes emptied of their water by drainage or evaporation **(Figs. 5a-b)** and develop as the newly-exposed lake floors undergo sub-aerial freezing, either diurnally or seasonally. Iteratively, this engenders the downward propagation and aggradation of permafrost, impelling pore-water away from the freezing fronts and towards the remaining pockets of unfrozen ground (e.g. Mackay, 1998, 1999; Walker and Jorgenson, 2011) **(Fig. 5a)**. As the hydrostatic pressure of the pore-water increases, the sedimentary overburden, i.e. formerly, the lake floor, begins to deform and uplift, creating a dome-like mound **(Figs. 5b-c)**. As the pore-water freezes an ice core forms **(Figs. 5a, e)**.

Pingo heights range from metres **(Fig. 5c)** to decametres **(Fig. 5d)** and long axes may reach hundreds of metres **(Fig. 2e)** (e.g. Washburn, 1973; Mackay, 1998, 1999; French, 2007). Pingo shape, usually circular to sub-circular **(Figs. 2e, 5b-d)**, is determined by the morphology or bathymetry of the lake floors or basins in which they are nested (e.g. Washburn, 1973; Mackay, 1998, 1999; French, 2007).

Amongst larger pingos, metres wide and deep fissures, i.e. dilation cracks, are not unusual **(Figs. 2e, 5d)**. These cracks propagate and trend from the mound summit as the pingo grows and tensile stresses increase within the sedimentary overburden (e.g. Washburn, 1973; Mackay, 1998, 1999; French, 2007). Sometimes, these cracks grade into the surrounding polygonised terrain (Mackay, 1998).

As the cracks widen and deepen, the ice core's sedimentary overburden stretches and thins. This increases the likelihood of thaw penetration, thermal instability and the subsequent formation of a summit depression or pit as the ice core ablates **(Figs. 2e; 5d)** (Mackay, 1998**)**. The ongoing exposure of the ice core to thaw may engender thaw slumps and/or small-scale debris flows. A slightly-elevated, sometimes irregular rampart represents the end-stage of pingo evolution (**Fig. 5g)** (Mackay, 1998). Amassed debris sometimes covers these ramparts (Washburn, 1973).

4.2 Ice complexes

Ice complexes comprise metre- to decametre-thick sequences or horizons of fine-grained, ice-rich sediments that have accumulated by means of fluvial, glacial, fluvio-glacial or aeolian processes **(Figs. 6a-i)**. Ice-enrichment occurred during the disparate warming periods of the Holocene Epoch. Invariably, the periglacial regions populated by the *CSPs* also exhibit ice complexes and cryologically-related landforms, i.e. thermokarst and alases, ice veins and ice-wedge polygons, beaded-drainage networks, etc (the *TC*: Rampton and Bouchard, 1974; Rampton,

188 1988; French, 2007; Grosse et al., 2007; Morgenstern et al., 2007, 2013; Schirrmeister et al., 2002,
189 2013; and northeast Russia: e.g. Czudek and Demek, 1970; Schirrmeister et al., 2002, 2013; Grosse
190 et al., 2007).

191 Permafrost is *ice-rich* if and when it contains *excess ice*, i.e. the volume of ice in the ground
192 that exceeds the total pore-volume that the ground would have under unfrozen conditions (e.g.
193 Harris et al., 1988; also, see Taber, 1930; Penner, 1959; Rampton and Mackay, 1971; Washburn,
194 1973; Murton, 1996; Rampton, 1988; French, 2007). Excess ice may comprise ice lenses, veins,
195 wedges or larger masses of consolidated ice formed by ice segregation. Fine to medium-grained
196 soils such as silts or silty clays are particularly adept at hosting segregation ice because they have
197 relatively-small interstices. Small interstices facilitate the migration of pore water by cryosuction
198 and the formation of discrete layers or lenses of *segregation ice* at the freezing front (Taber, 1930;
199 Penner, 1959; Rampton and Mackay, 1971; Rampton, 1988; French, 2007).

200 *Thermokarst* refers to terrain in regions of *ice-rich* permafrost that undergoes frost heave
201 and settlement in response to the volumetric aggradation or degradation of *excess ice*. Frost heave
202 occurs as segregated-ice forms and aggrades (Taber, 1930; Penner, 1959; Rampton, 1988). Frost
203 settlement occurs when segregation-ice thaws or degrades and the host terrain settles under its own
204 weight until it reaches a consolidated state (Harris et al., 1988). Frost heave and settlement occur
205 seldomly where the terrain is ice poor and exhibits only ice cement between sedimentary grains
206 (Péwé, 1954).

207 Thaw-derived meltwater may pool; this creates a transient lake or pond. The total loss of
208 lake or pond water by drainage or evaporation engenders the formation of a thermokarstic
209 depression absent of water, i.e. an alas (Washburn, 1973; Rampton, 1988; French, 2007). If the
210 loss is partial and episodic, then inwardly-oriented benches or terraces may develop on the alas

margins; this would give the margins a distinctly-scalloped appearance (e.g. Brown et al., 1981; Soare et al., 2008, 2011).

Spatially, the formation of thermokarst lakes and alases in an ice-rich landscape delineate the depth, breadth and scale of thermal disequilibrium, i.e. the sustained rise of sub-aerial mean (summer) temperatures (e.g. Péwe, 1954; Anderson and Hussey, 1963; French, 2007; Grosse et al., 2007; Schirrmeister et al., 2013; Wetterich et al., 2014), as well as ice loss (e.g. Czudek and Demek, 1970; Rampton and Mackay, 1971; Washburn, 1973, Rampton, 1988; French, 2007). Alas valleys, individual depressions that have conjoined as they have grown over time, comprise kilometres of reach and are meso-scale markers of thermal disequilibrium in an ice-rich landscape (e.g. Czudek and Demek, 1970; French, 2007).

4.3 Polygonised terrain

Small-sized (generally ≤25 m in diameter) and non-sorted polygons are observed wherever thermokarst landforms populate the landscape (e.g. Lachenbruch, 1962; Mackay, 1972; 1999; Czudek and Demek 1970; Rampton and Bouchard 1974; Rampton, 1988; French, 2007) **(Figs. 6c-e)**. The polygons are produced by the tensile-induced fracturing that arises from the sharp drop of sub-zero (0°C) temperatures in frozen ground (Lachenbruch 1962). This fracturing, referred to as *thermal-contraction* cracking, initially forms shallow vertical and horizontal fissures or cracks that are scattered across the landscape.

Crack fill, depending on the ambient environmental-conditions and the relative availability of atmospheric, surface/near-surface water, or of wind-blown soil/sand, comprises one of three types. **1)** Seasonally-produced meltwater derived of thawed snow or ice, ubiquitous in the relatively mild and humid Tuktoyaktuk Coastlands **(Figs. 6c, g)**; **2)** winter hoarfrost; and, **3)** windblown sand **(Figs. 6f-g)**, mineral-soil, or a mixture of the two (e.g. de Leffingwell 1915; Péwé

1959; Lachenbruch 1962; Washburn 1973; Sletten et al. 2003; Hallet et al. 2011). The seasonal iteration of thermally-induced cracking and crack filling eventually modifies the shallow and narrow veins into deeper and wider cracks. As thermal-contraction cracks propagate through a landscape they intersect and form polygon networks, often on a multi-kilometre scale (e.g. Black 1952; Lachenbruch 1962; Washburn 1973; Mackay 1974) **(Figs. 6d-e)**. Typically, the diameters of thermal-contraction cracks range from ~5-40 m (Washburn 1973; French 2007).

If underlain by aggrading ice-wedges then the polygon margins may display raised shoulders, relative to the polygon centres or to the terrain's elevation-datum, and are referenced as *low-centred polygons* (*LCPs*) (Washburn 1973; Harris et al., 1988; Rampton, 1988; French 2007; **Fig. 6e)**. Ice-wedges undergoing thaw (degradation) may exhibit collapsed shoulders, relative to the polygon centres, and are referenced as *high-centred polygons* (*HCPs*) (Washburn 1973; Harris et al., 1988; Rampton, 1988; French 2007) **Figs. 6c-g)**. Spatially-associated assemblages of *LCPs*/*HCPs* are not uncommon wherever closed-system pingos are observed and, as with the presence of thermokarst in a landscape, denote the ubiquity of liquid water and of active freeze-thaw cycling on a local if not a regional scale (e.g. Rampton and Bouchard, 1974; Rampton, 1988; Mackay, 1972, 1974).

Sand-wedge polygons (*SWPs*) also are observed in thermokarst landscapes (e.g. Mackay and Matthews, 1983; Murton et al., 2000) **(Figs. 6f-g)**. They are paleo-markers of climatic, hydrological and aeolian regimes that differ markedly, i.e. drier and/or colder, from the regimes associated with the origin and development of ice-wedge polygons, i.e. slightly warmer, wetter and less active, be they *LCPs* or *HCPs* (Washburn, 1973; Mackay and Matthews, 1983; Murton et al., 2000; Wolfe et al., 2018).

Morphologically, the variance of relative elevation between polygon centres and margins that arises when ice wedges aggrade or degrade is more subtle or muted in the case of the *SWPs*. This is to be expected. The volumetric gain or loss of soil space engendered by the freeze-thaw cycling (ice-wedge aggradation/degradation) is greater (+/-9%) than the gain or loss of soil space when sand is added or removed from a wedge site. Moreover, the volumetric potential of water to migrate from a thaw zone by means of surface or through flow is higher than the potential of sand to be removed from a wedge site purely by the work of wind.

Outcrops of low and high-centred sand-wedge polygons, albeit spatially-disassociated, also develop in the extreme aridity and low temperatures of the McMurdo Dry Valleys *(MDVs*), Antarctica (e.g. Péwé, 1959; Lachenbruch, 1962; French and Guglielmin, 2000; Marchant et al., 2002; Sletten et al., 2003; Hallett et al., 2011). Here, similarly to the *LCPs* and *HCPs* that populate wet periglacial-landscapes in the northern hemisphere, the formation of both polygon types is initiated by thermal contraction (e.g. Péwé, 1959; Lachenbruch, 1962; French and Gugliemin, 2000; Marchant et al., 2002; Sletten et al., 2003; Hallett et al., 2011).

Further development also follows a similar path of aggradation and degradation, i.e. soil deforms upwardly (*LCPs*) as sandy wedge-fill accumulates by the work of wind and deforms downwardly (*LCPs*) as the sandy fill is removed from the wedge site by the work of wind (e.g. Péwé, 1959; Lachenbruch, 1962; French and Gugliemin, 2000; Marchant et al., 2002; Sletten et al., 2003; Hallett et al., 2011). Sometimes, development of the *HCPs* is enhanced by the sublimation of underlying glacial ice (Marchant et al., 2002).

Although ice-rich terrain within one metre of the surface has been reported in the *MDVs (*Lacelle et al., 2011, 2013), none of the locations where the *LCPs* or the *HCPs* are observed exhibit thermokarst, ice-wedging or beaded streams (French and Gugliemin, 2000; Marchant et al., 2002;

279 Sletten et al., 2003; Hallett et al., 2011). Moreover, whether or not the ice-rich terrain formed by
280 means of freeze-thaw or adsorption/diffusion cycles is unclear (Lacelle et al., 2011).

281 ***4.4 Small-scale "beaded-stream" systems***

282 Where ice wedges degrade and thaw, deflating raised polygon-shoulders below the
283 elevation datum of the polygon centres, marginal troughs or corner pits may form and collect ice-
284 wedge derived meltwater (e.g. Lawson, 1986; Walker and Jorgenson, 2011; Arp et al., 2012, 2015;
285 Tarbeeva and Surkov, 2013) **(Figs. 7a-d)**. Prolonged or iterative periods of thaw increase the
286 volume of meltwater in the troughs and pits, as well as in the surrounding terrain (Lachenbruch
287 1966; Arp et al., 2015).

288 Over time, the local topographical-gradient provides direction and drop for initially-
289 isolated pockets of meltwater to join (Anderson and Hussey, 1963; Arp et al., 2015; King et al.,
290 2016) **(Figs. 7a-b, d)**. This spatial coalescence forms the permafrost-based equivalent of a first-
291 order stream (Anderson and Hussey, 1963; Arp et al., 2012, 2015; Tarbeeva and Surkov, 2013)
292 whose reach eventually may comprise decametres to kilometres of surface coverage (Lawson,
293 1986; French, 2007; Walker and Jorgenson, 2011; Tarbeeva and Surkov, 2013) (**Figs. 7c-d)**.
294 Second, polygon-trough corners or junctions comprise multiple paths of possible meltwater-
295 migration and surface-flow, providing for higher rates of accumulation and thermal erosion than
296 linear or sub-linear marginal troughs. Thus, the junction pools exhibit greater depths to their floors
297 and surface areas than do the troughs (Péwé, 1954; Anderson and Hussey, 1963).

298 **5. A possible geochronology of *CSP* formation at the mid-latitudes of Utopia Planitia**

299 ***5.1 An icy origin***

300 Atmospherically precipitated ice/snow accumulates at the mid-latitudes of the northern
301 hemisphere, perhaps the result of Late Amazonian Epoch changes of obliquity and eccentricity

(e.g. Mustard et al., 2001; Head et al., 2003; Milliken et al., 2003; Morgenstern et al., 2007; Lefort et al., 2009; Madeleine et al. 2009; Séjourné et al., 2011). Remnants of the most recent atmospherically-precipitated mantle, possibly an icy one, are observed throughout the region (e.g. Mustard et al. 2001; Head et al., 2003; Milliken et al., 2003; Morgenstern et al., 2007; Schorghofer, 2007; Lefort et al., 2009; Soare et al., 2015; 2018a) **(Figs. 8a-c)**. The mantle shows a relatively-light tone (relative to the underlying terrain), smooth texture (at *HiRISE* resolution) and, often, is unpolygonised (Soare et al., 2015; 2018b-c).

A densely-cratered basement underlies the relatively dark and the light-toned terrains and is observed where overlying materials are relatively thin. The basement is old relative to the time scales of the recent obliquity and eccentricity changes **(Figs. 9a-c)**. Crater counts of visible rims from this underlying surface indicate the crater population is in saturation equilibrium. This is consistent with a Noachian-aged surface. However, the overlying darker-toned material is cratered sparsely. The size-frequency distribution of the craters is indicative of a surface that has been modified as it has a shallow power-law slope. This is the consequence of fewer meter-to-decametre scale craters than predicted from crater-production functions (e.g. Hartmann, 2005). The number of ~100 m craters, contrarily, precludes a surface younger than ~100 Ma. The craters on this surface have a subdued, shallow appearance, lacking rims and ejecta similar to the heavily-degraded craters, or hollows, observed by the Mars Exploration Rovers (e.g. Grant et al., 2006; Golombek et al., 2014). Thus, the low density of craters is the result of crater degradation and is not indicative of a youthful surface (e.g. Smith et al., 2008; Kite and Mayer, 2017; Williams et al., 2018). From this, we can infer that the age probably is not younger than ~100 Ma, although an absolute age cannot be derived.

5.2 Periglacial revisions and the collapse of thermokarst

A less-than-recent icy mantle (unobserved but inferred from the cyclical nature of mantle formation (e.g. Mustard et al.., 2001; Head et al., 2003; Milliken et al., 2003; Schorghofer, 2007; Madeleine et al., 2009) undergoes freeze-thaw cycling of ice/snow. Meltwater migrates through the relatively dark-toned and possibly fine-grained volcanic regolith to depth (Soare et al., 2015). Excess ice develops, i.e. ice lenses, veins, wedges or larger masses of consolidated ice, as the meltwater undergoes freeze-thaw cycling (Sizemore et al., 2015; Soare et al., 2015; 2018) and thermokarst forms (Soare et al., 2018a, b).

Blanketed by a sublimation lag, the thermal integrity of thermokarst at the mid-latitudes is maintained for a period of time (e.g. Mellon and Jakosky, 1993; Mustard et al., 2001; Milliken et al., 2003; Dundas et al., 2015; Dundas, 2017). As the amplitude of mean surface-temperatures and atmospheric-humidity vary in response to cyclical changes of obliquity (Laskar and Robutel 1993; Touma and Wisdom 1993; Laskar et al., 2004), the near-surface excess ice sublimates; this mass loss triggers terrain deflation and, if sufficiently substantial, the formation of a thermokarstic depression (Dundas et al., 2015; Dundas, 2017). Inward-oriented benches or scarps **(Figs. 4a-b)** form in response to the episodicity of mass loss and comprise paleo-markers of individual periods of climate change (e.g. Morgenstern et al., 2007; Lefort et al., 2009; Ulrich et al, 2010; Séjourné et al., 2011; Soare et al., 2011, 2018a, b).

5.3 Polygonisation and beaded pit/trough assemblages

As the regional landscape undergoes this cryological evolution, thermal-contraction cracking polygonises the terrain episodically (e.g. Costard and Kargel, 1995; Seibert and Kargel, 2001; Morgenstern et al., 2007; Soare et al., 2008, 2011; Lefort et al., 2009; Levy et al., 2009; Madeleine et al. 2009; Ulrich et al., 2010; Séjourné et al., 2011) **(Fig. 4)**. Differences in the structural complexity of the polygon networks, i.e. the density of secondary vs primary cracks in

a polygon and or the disparity between polygon diameters within the depressions and those observed without, are paleo-markers of this episodicity (Lefort et al., 2009; Ulrich et al., 2010; Séjourné et al., 2011).

Some of the polygons exhibit high centres, relative to their margins; elsewhere, the polygons express low centres, relative to their margins **(Figs. 4d-e)**. Differences in polygon centre-margin morphologies are not an unequivocal marker of ice-wedging, as disparate non-icy types of fill could underlie raised or lowered polygon margins **(Figs. 6f-g)**.

However, if the two polygon types are observed in the midst of landscapes that exhibit a multiplicity of geological weaves with possible ice-richness and the freeze-thaw cycling of water, then deducing an ice-wedge origin for the *lcps* or *hcps* is not unjustifiable (Wan Bun Tseung and Soare, 2006; Soare, Conway and Dohm 2014; Soare et al. 2018a). This is the case especially where *lcps* and *hcps* are observed in proximity, as the origin of the two distinct but spatially-associated polygon-morphologies or types could be explained most simply by transient (triple-point of water) boundary conditions.

Similarly, the small-scale and spatially-associated polygon-margin troughs and corner pits that are observed within and without the rimless and sometimes scalloped depressions could be the degradational artefacts of ice-wedging **(Figs. 4b-c)**. In other words, as the near-surface ice wedges sublimate, cavities or voids develop in the regolith; this engenders the deflation or collapse of the overburden (Wan Bun Tseung and Soare, 2006, Séjourné et al., 2010; 2011; Soare et al., 2011, Glines and Gulick, 2018; also, Costard et al., 2016). Collectively, the beaded appearance and spatial connectivity of the troughs and corner pits are similar to that which is observed on Earth wherever thermokarst and ice wedges are undergoing the loss of thermal integrity (Wan Bun Tseung and Soare, 2006, Soare et al., 2011, Costard et al., 2016; Glines and Gulick, 2018).

371 The dominant topographical-gradient in *UP* is east-west. However, there is a more subtle
372 downslope trend that runs from the southern highlands to the pole (e.g. Zuber et al., 1998;
373 Hiesinger and Head, 2000), especially where the polygonised terrain is observed (Hiesinger and
374 Head, 2000). The alignment of the polygon troughs and pits is consistent with the second gradient.

375 ***5.4 Ice mound formation***

376 Warming conditions, driven by recent changes of obliquity and eccentricity and facilitated,
377 perhaps, by the presence of brines in the regolith (e.g. Primm et al., 2017; Jones, 2018), induces
378 the: **a)** thaw of residual excess-ice in the near surface; and, **b)** pooling of meltwater beneath the
379 scalloped terrain. Subsequent freezing-conditions trigger permafrost aggradation in the near-
380 surface of the scalloped terrain, promoting the growth of an ice-cored mound. Dilation cracks form
381 at the summit as the overburden stretches with mound growth. The cracks may grade radially
382 towards the surrounding terrain and, as in pingo-dotted landscapes on Earth, intercept the polygons
383 surrounding them. Summit depressions and elevationally-depleted mound centres also are
384 observed **(Figs. 2a-b; 3a-d)**; they may be markers of ice-core degradation as regional temperatures
385 rise and the active layer deepens.

386 **6. Non-periglacial origins of the rimless and sometimes scalloped depressions and mounds?**

387 *6.1 Thermokarst and sublimation?*

388 Within the community of Mars planetary-researchers there is a widespread agreement that
389 the rimless and sometimes scalloped depressions at the mid-latitudes of *UP* are thermokarst (e.g.
390 Costard and Kargel, 1995; Seibert and Kargel, 2001; Morgenstern et al., 2007; Soare et al., 2008,
391 2018a,b; Lefort et al., 2009; Ulrich et al., 2010; Séjourné et al., 2011; Dundas et al., 2015; Dundas,
392 2017). No less widespread is the belief that the loss of excess ice probably is the work of
393 sublimation (e.g. Costard and Kargel, 1995; Seibert and Kargel, 2001; Morgenstern et al., 2007;

394 Soare et al., 2018a,b; Lefort et al., 2009; Ulrich et al., 2010; Séjourné et al., 2011; Dundas et al.,
395 2015; Dundas, 2017).

396 The *MDVs* in the Antarctic exhibit some icy landscape-features that could have been
397 revised by sublimation (e.g. Marchant et al., 2002; Kowaleski et al., 2006; Lacelle et al., 2011,
398 2013). For example, buried and ancient glacial-ice in Beacon Valley, one of the *MDVs*, may
399 undergo highly-localised sublimation where the terrain is incised by thermal-contraction cracking
400 and the cracks migrate through polygon troughs in the glacial overburden to the underlying ice. At
401 the University Valley, adjacent to the Beacon Valley, water vapour condensation/diffusion is
402 invoked to explain the past formation of excess ice in the upper few centimetres of the soil as
403 seasonal temperatures and atmospheric vapour-pressures have varied seasonally within the last
404 ~135 ka (Lacelle et al., 2011, 2013).

405 The sub-metre horizons of the excess ice in the *MDVs* are significantly thinner, by at least
406 two orders of magnitude (Lacelle et al., 2011, 2013), than the deepest thermokarst-like depressions
407 on Mars. This could be an empirical constraint, in as much as sublimation-tolerant conditions occur
408 for significantly shorter time periods on Earth than on Mars; or, there could be a theoretical
409 constraint on the propagation depths of adsorption/diffusion cycles. Modelling shows that the
410 accumulation of adsorbed ice in the near-surface pore space would choke the subsequential transfer
411 of vapour to lower layers (Clifford, 1993; Mellon and Jakosky, 1993; also, Dundas et al., 2015).
412 Either way, most thermokarst landscapes and ice complexes on Earth have evolved in
413 environments largely absent of sublimation (Dundas et al., 2015).

414 On the other hand, there is no inconsistency in hypothesising a freeze-thaw origin for
415 excess ice and thermokarst (Soare et al., 2017, 2018a, b), be it on Earth or on Mars, while
416 acknowledging that sublimation is responsible for the voiding of excess ice in the near-surface

417 wherever the thermokarstic depressions are observed in our study region. The former assumes
418 slightly different triple-point conditions than the latter, and defers to the only recognised means by
419 which excess ice could form to decametres of depth.

420 *6.2 The pingo-like mounds*

421 Numerous researchers have reported the possible presence of kilometre-and sub-kilometre
422 scale pingos in Utopia Planitia and have evaluated disparate formation-hypotheses for the
423 candidate mounds (Morgenstern et al., 2007; Osinski and Soare, 2007; Dundas et al., 2008; Burr
424 et al., 2009; de Pablo and Komatsu, 2009; Soare and Osinski, 2009; Dundas and McEwen, 2010;
425 Soare et al., 2013a). Here, we describe, discuss and contrast two sub-kilometre mound-types that
426 share the greatest number of similarities with closed-system pingos on Earth, **a)** intra-crater,
427 variable in shape and banded; and, **b)** flat topped, typically circular and fractured. These two
428 mound-types are commonplace in the region studied by us and often occur in close spatial-
429 association with the mounds interpreted by us to be *CSPs*. For a broader discussion of all small-
430 scale mound types in the region, see Burr et al., (2009).

431 *6.2.1 Intra-crater mounds (ICMs)*

432 Sub-kilometre mounds rooted in kilometre-and sub-kilometre scale impact craters **(Figs.**
433 **10a-b)** are ubiquitous at the mid latitudes of *UP* (Soare et al., 2013; also, Morgenstern et al., 2007;
434 Osinski and Soare, 2007; Soare and Osinski, 2009; Dundas and McEwen, 2010). Mound
435 morphologies are wide-ranging, i.e. circular and sub-circular to crescentic, and, distribution,
436 generally, is clustered **(Fig. 10a)** (Soare et al., 2013; also, Soare and Osinski, 2009; Dundas and
437 McEwen, 2010). Volumetrically, the ratio of mound-surface to crater-basin area varies from high
438 (basin filling) to low (barely observable) (Dundas and McEwen, 2010; Soare et al., 2013a) **(Fig.**
439 **10a)**. Some of the mounds show metre to decametre-scale (in elevation) single or multiple terraces,

immediately adjacent to but topographically lower than the mound summits **(Figs. 10a-b)**. This could be indicative of differential accumulation and erosion derived of texturally-disparate strata, i.e. loess, ice dust or volcanic sediments (Soare et al., 2013a).

Some of the mound summits are domed (**Fig. 10b)**; some of them show metres-scale pitting, as does the terrain adjacent to the mounds on the crater floor (Dundas and McEwen, 2010) **(Figs. 10a-b)**. Contrarily, neither the mounds nor the adjacent terrain are polygonised (Soare and Osinski, 2009). However, where the crater-nested mounds are observed within the thermokarstic depressions, the adjacent terrain may show polygonisation (Soare and Osinski, 2009).

6.2.2 Flat-topped mounds (FTMs)

Sub kilometre mounds that are circular to sub-circular with flat mesa-like summits and steep sides are ubiquitous in the region, often in terrain shared with the *ICMs* (Dundas et al., 2008; Dundas and McEwen, 2010; **Figs. 11a-d)**. Some of the mounds display multiple fractures, one or two of which may be prominent, i.e. slightly wider and deeper than the others (Dundas and McEwen, 2010). Many of the fractures are diametrical and some of the fractures extend to the surrounding terrain, intersecting polygons incised therein **(Figs. 11b-c)**. The *FTMs* are observed in polygonised or in metre-scale pitted terrain and they themselves may be pitted. None of the observed mounds, however, exhibit the substantial variance of shape associated with the *ICMs*. Nor do they show the range of possible degradational features associated with the candidate *CSPs*.

7. A periglacial origin?

7.1 Martian pingos and periglaciation

We propose that the geological, geomorphological and analogue-derived fit between *wet-based* periglaciation and the candidate *CSPs* is closer and more plausible than the alternatives:

462 **a)** It is generally agreed that the flat-floored, rimless and sometimes scalloped depressions
463 at the mid-latitudes of *UP* are thermokarstic and that they are embedded in ice-rich
464 terrain to depth. On Earth, ice-rich terrain to depth occurs only where liquid water is
465 abundant at or near the surface and where the freeze-thaw cycling of this water
466 dominates (or has dominated) the regional landscape.

467 **b)** Whether or not the polygons in the region are underlain by ice or sand wedges is open-
468 ended. However, the following geological constraints favour an origin based on the
469 freeze-thaw cycling of water. First, the spatial synonymy of the polygons with the
470 thermokarst-like and possibly ice-rich or depleted depressions. Second, the adjacency
471 of *lcps* and *hcps* at some candidate *CSP* sites, possibly suggesting transitional albeit
472 highly localised triple-point conditions. Third, spatial assemblages of polygon-margin
473 troughs and corner pits. In permafrost regions on Earth similar assemblages point to
474 the episodic thaw of ice-wedge polygons, sometimes on a regional scale.

475 **c)** In addition to being nested in thermokarstic depressions the Martian mounds show
476 synonymy with *CSPs* on Earth across a broad spectrum of geological traits and
477 landscape features: similarity of scale and shape, domed summits, summit depressions
478 and summit fractures, possible degradation and end-stage morphologies; adjacency to
479 polygonised terrain (that may comprise *LCPs* and/or *HCPs*) and to polygon-margin
480 troughs and corner pits that could be analogous to beaded-stream systems.

481 **7.2 Alternatives**

482 We propose that the dissimilarities between the *ICMs* and the candidate *CSPs* in *UP,* let
483 alone between the *ICMs* in *UP* and *CSPs* on Earth, are sufficiently abundant to discount a
484 periglacial origin for the former.

First, the *ICMs* exhibit intra-crater morphologies that vary from almost crater-filling to crescentic, with the latter often being observed in the eastern/northeastern quadrant of the mound-bearing impact craters (Soare et al., 2013a). The suggestion has been made that the large range or variance of morphologies associated with the *ICMs* could be the result of sedimentary accumulation and aeolian erosion, possibly dominated by prevailing winds from the southeast (Soare et al., 2013a; Steele et al., 2018). The candidate *CSPs* exhibit no similarity of morphological range or variance or more than one level of terracing.

Second, the relatively-pristine shape of the crescentic *ICMs* and their terraces, i.e. being unbroken or modified by slumping or debris flows, points away from the possible presence of a buried or underlying ice-core. Were the *ICMs* actually ice-cored mounds overlain by sediments, the stripping away of the sedimentary overburden by aeolian activity would increase the ice-core's sensitivity to ablation. As the ice-core ablates the loss of mass would engender the collapse of the core overburden. This, in turn, would initiate small-scale slumping and debris flows (Mackay, 1998) **(Fig. 6c)**. No apparent debris flows or slumps, however, are observed either on the terraces or the slopes of the *ICMs*.

The *FTMs*, by contrast, share a number of traits with the candidate *CSPs*. First, they exhibit similarities of scale and, often, of circular or sub-circular shape. Second, they are incised by diametrical cracks or fissures. Third, they are observed, although not exclusively, in polygonised terrain. On the other hand **1)** the range of morphologies possibly associated with ice-core degradation are absent from the *FTMs*, as they are with the *ICMs*; and, **2)** the *FTMs* are observed, almost exclusively, away from the thermokarstic depressions and, sometimes, in terrain that is unpolygonised and absent of the polygon-margin and corner-pit depression assemblages.

8. Discussion and Conclusion

508 *8.1 Ice-rich terrain and the freeze-thaw cycling of water on Mars*

509 As early as the Mariner missions fifty years or so ago Mars-focused planetary scientists
510 noted that the partial pressure of water vapour at the surface of Mars generally is below the triple
511 point of water (e.g. Anderson et al., 1967; Sharp et al., 1971; Sharp, 1973). In as much as the origin
512 and development of ice-rich landscape complexes require water stability or, minimally, iterative
513 meta-stability, this was troubling for scientists reporting ice-complex like features and landforms
514 on Mars (e.g. Anderson et al., 1967; Sharp et al., 1971; Sharp, 1973; Lucchitta, 1981; Theilig and
515 Greeley, 1979; Rossbacher and Judson, 1981).

516 However, well before the recent observations and experimental findings about briny
517 freezing-point depressants at/near the Martian surface and diurnal temperatures/pressures above
518 the triple point at all Martian latitudes (e.g. Haberle et al., 2001; Hecht, 2002; Chevrier et al., 2009;
519 Chevrier et al., 2012; Ohja et al., 2015; Primm et al. 2017; Jones, 2018), it was thought that
520 diliquescent salts or brines could:

521 **a)** enhance the water-vapour sorption capacity of soil (Anderson et al., 1967, also,
522 Rossbacher and Judson, 1981), especially if that soil comprises relatively small-grains,
523 i.e. clays (Anderson et al., 1967); and,

524 **b)** facilitate the development of ice-rich *thermokarst*, i.e. terrain that swells and contracts
525 as ice lenses form and sublimate or evaporate (e.g. Anderson et al., 1967; Sharp et al.,
526 1971; Sharp, 1973; Lucchitta, 1981).

527 It should also be noted that *wet* periglacial-landscapes on Earth form episodically and that
528 the stability of liquid water where this happens need not be exhibited uniformly through the course
529 of a calendar year. Favourable boundary-conditions expressed for a few hours diurnally and
530 seasonally suffice. For example, in 1978 Mackay (1997, 1999) drained a thermokarst lake

531 artificially at Richards' Island in the *TC*. Within six years of this drainage, and through the
532 accompanying diurnal/seasonal periods of thaw-freeze cycling, he observed the origin and
533 development of metre-sized mounds with radii from ~15-25 m and small ice-wedge polygons
534 beginning to form on the lake floor (Mackay, 1997, 1999).

535 *8.2 Remote reasoning*

536 Absent of boots on the ground and a pick or shovel, the attempt to validate the *CSP*
537 hypothesis requires deducing process from landscape and moving probabilistically between Earth
538 and Mars-based geological systems:

539 **a)** Broadly speaking, the proposed geochronology of landscape evolution at the mid-
540 latitudes of *UP*, as well as the need for icy material to initiate the freeze-thaw cycling
541 of water at the mid-latitudes where the candidate *CSPs* are observed, are in line with
542 recent work on obliquity-driven atmospheric precipitation and surface accumulation.

543 **b)** Even in the light of current Martian boundary-condition, the temperature and pressure
544 requirements of water undergoing episodic freeze-thaw cycling in our study region are
545 not implausible. This is true particularly under a soil regime where brines are
546 commonplace (e.g. Jones, 2018) and diurnal periods of meta-stability are hours-long
547 (Primm et al., 2017).

548 **c)** The relative location of the candidate *CSPs* within the rimless and sometimes scalloped
549 depressions, as well as the similarity between the *UP* mounds and terrestrial *CSPs* in
550 scale, height, shape, range of shape variance, surface fractures, domed summits,
551 summit depressions, polygonisation, proximity to assemblages of linear and beaded
552 polygon-margins, and fracturing, are consistent with a "*wet*" periglacial origin.

553 In and of themselves, some of the geological predicates identified above need not be the
554 product of water undergoing freeze-thaw cycling, i.e., **a)** polygons whose margins are underlain
555 by sand; or, **b)** the thermokarst-like depressions being devolatilised by sublimation, etc. Occam's
556 razor, however, points in another direction. On the other hand, the origin and development of the
557 candidate *CSPs* in *UP* is explained most simply by a tightly-weaved set of geological observations
558 and a landscape-scale hypothesis driven by a single process, i.e. the freeze-thaw cycling of water.
559 Alternative explanations, while "*drier*" and possibly credible on lesser scales of analysis, lack the
560 overall robustness of a "*wetter*" hypothesis.

561 **References**

562 Anderson, D.M., Gaffney, E.S., Low, P.F., 1967. Frost phenomena on Mars. Science 155, 3760,
563 319-322, doi:10.1126/science.155.3760.319.

564 Anderson, G.S., Hussey, K.M., 1963. Preliminary Investigation of Thermokarst Development on
565 the North Slope, Alaska. Proceedings of the Iowa Academy of Science 70, 55, 306-320.

566 Arp, C.D., Whitman, M.S., Jones, B.M., Kemnitz, R., Grosse, G., Urban, F.E., 2012. Drainage
567 network structure and hydrologic behavior of three lake-rich watersheds on the Arctic
568 Coastal Plain, Alaska. Arctic, Antarctic, and Alpine Research 44, 4, 385-398, doi.org/10.
569 1657/1938-4246-44.4.385.

570 Arp, .C.D. Whitman, M.S., Jones, B.M., Grosse, G., Gaglioti, B.V., Hei, K.C., 2015. Distribution
571 and biophysical processes of beaded streams in Arctic permafrost landscapes.
572 Biogeosciences, 12, 29-47, doi:10.5194/bg-12-29-2015.

573 Black, R.F., 1952. Polygonal patterns and ground conditions from aerial photographs.
574 Photogrammetric Engineering 18, 1, 123-134.

575 Brown, R.J.E., Johnston, G.H., Mackay, J.R., Morgenstern, N.R., Shilts, W.W., 1981. Permafrost

576 distribution and terrain characteristics, in (ed.) G.H. Johnson, Permafrost, Engineering
577 Design and Construction, 31-72.
578 Burr, D.M., Soare, R.J., Wan-Bun Tseung, J.M., Emery, J.P., 2005. Young (late Amazonian) near-
579 surface ground-ice features near the equator. Icarus 178, 1, 56-73, doi.org/10.1016/2005.
580 04.012.
581 Burr, D.M., Bruno, B.C., Lanagan, P.D., Glaze, L.S., Jaeger, W.L., Soare, R.J., Wan Bun Tseung,
582 J-M., Skinner, J.S., Baloga, S.M., 2009. Mesoscale raised rim depressions (MRRDs) on
583 Earth: A review of the characteristics, processes, and spatial distributions of analogs for
584 Mars. Planetary and Space Science 57, 479-596, doi:10.1016/j.pss.2008.11.011.
585 Cabot, E.C., 1947. The Northern Alaskan Coastal Plain interpreted from aerial photographs.
586 Geographical Review 37, 4, 639-648.
587 Chevrier, V.F., Hanley, J., Altheide, T.S., 2009. Stability of perchlorate hydrates and their liquid
588 solutions at the Phoenix landing site, Mars. Geophysical Research Letters 36, L10202,
589 doi.org/10.1029/2009GL037497.
590 Chevrier, V.F., Rivera-Valentin, E.G., 2012. Formation of recurring slope lineae by liquid brines
591 on present-day Mars, 39, L21202, doi.org/10.1029/2012GL054119
592 Clifford, S.M., 1993. A Model for the hydrologic and climatic behavior of water on Mars.
593 Journal of Geophysical Research 98, E6, 10,973-11,106.
594 Christensen, P.R., et al. 2004. The Thermal Emission Imaging System (THEMIS) for the Mars
595 Odyssey mission. Space Science Review, 110, 85-130.
596 Costard, F., Kargel, J.S., 1995. Outwash plains and thermokarst on Mars. Icarus 114, 93-112.
597 Costard, F., Séjourné, A., Kargel, J.S., Godin, E., 2016. Modeling and observational occurrences

598 of near-surface drainage in Utopia Planitia, Mars. Geomorphology 275, 80-89,
599 dx.doi.org/10.1016/j.geomorph.2016.09.034.
600 Czudek, T., Demek, J., 1970. Thermokarst in Siberia and its influence on the development of
601 lowland relief. Quaternary Research 1, 103-120.
602 De K Leffingwell, E. 1915. The Canning River Region, Northern Alaska. USGS Professional
603 Paper 109, 251 p.
604 de Pablo, M.A., Komatsu, G., 2009. Possible pingo fields in the Utopia basin, Mars: Geological
605 and climatical implications. Icarus 199, 1, 49-74, doi.org/10.1016/j.icarus.2008.09.007.
606 Dundas, C.M., 2017. Effects of varying obliquity on Martian sublimation thermokarst landforms.
607 Icarus 281, 115-120, dx.doi.org/10.1016/j.icarus.2016.08.031.
608 Dundas, C.M., Byrne, S., 2010. Modeling sublimation of ice exposed by new impacts in the
609 martian mid-latitudes. Icarus 206, 716-728, doi:10.1016/j.icarus.2009.09.007.
610 Dundas, C.M., McEwen, A.S., 2010. An assessment of evidence for pingos on Mars using
611 HiRISE. Icarus 205, 244-258, doi:10.1016/j.icarus.2009.02.020.
612 Dundas, C.M., Mellon, M.T., McEwen, A.S., Lefort, A., Keszthelyi, L.P., Thomas, N., 2008.
613 HiRISE observations of fractured mounds: Possible martian pingos. Geophysical Research
614 Letters 35, L04201, doi.org/10.1029/2007GL031798.
615 Dundas, C.M., Byrne, S., McEwen, A.S., 2015. Modeling the development of martian sublimation
616 thermokarst landforms. Icarus 262, 154-169, dx.doi.org/10.1016/j.icarus.2015.07.033.
617 French, H.M., Guglielmin, M., 2000. Frozen ground phenomena in the vicinity of Terra Nova
618 Bay, Northern Victoria land, Antarctica: a preliminary report. Geografiska Annaler ·82 A,
619 513-526.
620 French, H.M., 2007. The periglacial environment, West Sussex, England, J. Wiley & Sons, 458

621 p.
622 Glines, N.H., Gulick, V.C., 2018. Thermokarst paleolake assemblages and channels in Lyot
623 Crater, Mars. 49th LPSC, abstract # 2955, Houston, Texas.
624 Golombek, M.P., Warner, N.H., Ganti, V., Lamb, M.P., Parker, T.J., Fergason, R.L., Sullivan. R.,
625 2014. Small crater modification on Meridiani Planum and implications for erosion rates
626 and climate change on Mars, Journal of Geophysical Research, 119, 2522-2547, doi:10.
627 1002/2014JE004658.
628 Grant, J.A., et al. 2006. Crater gradation in Gusev crater and Meridiani Planum, Mars, Journal of
629 Geophysical Research, 111, E02S08, doi:10.1029/2005JE002465.
630 Grosse, G., Schirrmeister, L., Siegert, C., Kunitsky, V.K., Slagoda, E.A., Andreev, A.A.,
631 Dereviagyn, Y., 2007. Geological and geomorphological evolution of a sedimentary
632 periglacial landscape in northeast Siberia during the late Quaternary. Geomorphology 86,
633 25-51, doi:10.1016/j.geomorph.2006.08.005.
634 Haberle, R.M., McKay, C.P., Schaeffer, J., Cabrol, N.A., Grin, E., Zent, A.P., Quinn, R., 2001.
635 On the possibility of liquid water on present day Mars. Journal of Geophysical Review
636 106, E10, 23,317-23,326.
637 Hallet, B., Sletten, R., Whilden, K., 2011. Micro-relief development in polygonal patterned
638 ground in the Dry Valleys of Antarctica. Quaternary Research 75, 347-355, doi.org/10.
639 1016/j.yqres.2010.12.009.
640 Harris, S.A., French, H.M., Heginbottom, J.A., Johnston, G.H., Ladanyi, B., Dego, D.C., van
641 Everingen, R.O., 1988. Technical Memorandum. 142, Permafrost Subcommittee, National
642 Research Council, 154 p.
643 Hartmann, W.K., 2005. Martian cratering 8: Isochron refinement and the chronology of Mars.

644 Icarus 174, 294-320, doi:10.1016/j.icarus.2004.11.023.
645 Head, J.W., Mustard, J.F., Kreslavsky, M.A., Milliken, R.E., Marchant, D.R., 2003. Recent ice
646 ages on Mars. Nature 426, 797-802, doi:10.1038/nature02114.
647 Hecht, M.H., 2002. Metastability of liquid water on Mars. Icarus 156, 373-386, doi:10.1006/icar.
648 2001.6794.
649 Hecht, M.H., 2009. Detection of Perchlorate and the Soluble Chemistry of Martian Soil at the
650 Phoenix Lander Site. Science 325, 5936, 64-67, doi:10.1126/science.1172 466.
651 Hiesinger, H., Head, J.W., 2000. Characteristics and origin of polygonal terrain in southern Utopia
652 Planitia, Mars: Results from Mars Orbiter Laser Altimeter and Mars Orbiter Camera data.
653 Journal of Geophysical Research 105, E5, 11,999-12,022.
654 Hinkel. K.M., Frohn, R.C., Nelson, F.E., Eisner, W.R., Beck, R.A., 2005. Morphometric and
655 spatial analysis of thaw lakes and drained thaw lake basins in the Western Arctic Coastal
656 Plain, Alaska. Permafrost and Periglacial Processes 16, 327-341, doi:10.1002/ ppp.532.
657 Jones, E., 2018. Shallow transient liquid water environments on present-day Mars, and their
658 implications for life. Acta Astronautica 146, 144-150, doi.org/10.1016/j.actaastro.2018.02.
659 027.
660 Kite E.S., Mayer D.P., 2017. Mars sedimentary rock erosion rates constrained using crater counts,
661 with applications to organic-matter preservation and to the global dust cycle. Icarus
662 286:212-222, doi.org/10.1016/j.icarus.2016.10.010.
663 King, T.V., Neilson, B.T., Levi, Overbeck, L.D., Kane, D.L., 2016. Water temperature controls in
664 low arctic rivers, Water Resources Research 52, 4358-4376, doi:10.1002/2015WR017965.
665 Kneissl, T., van Gasselt, S., Neukum, G., 2011. Map-projection-independent crater size-frequency

666 determination in GIS environments - New software tool for ArcGIS. Planetary and Space
667 Science 59, 1243-1254, doi.org/10.1016/j.pss.2010.03.015.
668 Kowalewski, D.E., Marchant, D.R., Levy, J.S., Head, J.W., 2006. Quantifying low rates of
669 summer-time sublimation for buried glacier ice in Beacon Valley. Antarctica. Antarctic
670 Science 18 3, 421-428, doi:10.1016/j.geomorph.2010.11.001.
671 Lacelle, D., Davila, A.F., Fisher, D., DeWitt, R., Pollard, W.H., Andersen, D., Heldmann, J.,
672 Marinova, M.M., McKay, C.P., 2011. Vapour diffusion origin (condensation-adsorption)
673 in ice cemented permafrost spanning the last 135.5 ka years in University Valley, Dry
674 Valleys of Antarctica. 5th International Conference on Mars Polar Science and Exploration,
675 Fairbanks, Alaska, Abstract # 6083.
676 Lacelle, D., Davila, A.D., Fisher, D., Pollard, W.H., DeWitt, R., Heldmann, J., Marinova, M.M.,
677 McKay, C.P., 2013. Excess ground ice of condensation–diffusion origin in University
678 Valley, Dry Valleys of Antarctica: Evidence from isotope geochemistry and numerical
679 modeling. Geochimica et Cosmochimica Acta 120, 280-297, dx.doi.org/10.1016/j.gca.
680 2013.06.032.
681 Lachenbruch, A.H., 1962. Mechanics of thermal contraction cracks and ice-wedge polygons in
682 permafrost. GSA Special Paper 70. Geological Society of America, New York, 69 p.
683 Lachenbruch, A.H., 1966. Contraction theory of ice-wedge polygons: a qualitative discussion,
684 Permaforst International Conference, Lafayette, Indiana, 63-70.
685 Laskar, J., Correia, A.C.M., Gastineau, M., Joutel, F., Levrard, B., Robutel, P., 2004. Long term
686 evolution and chaotic diffusion of the insolation quantities of Mars. Icarus 170, 343-364,
687 doi.org/10.1016/j.icarus.2004.04.005.
688 Laskar, J., Robutel, P., 1993. The chaotic obliquity of the planets. Nature 361, 608-612.

689 Lawson, D.E., 1986. Response of permafrost terrain to disturbance: a synthesis of observations
690 from Northern Alaska, U.S.A. Arctic and Alpine Research 18, 1, 1-17.
691 Lefort, A. Russell, P.S., Thomas, N., McEwen, A.S., Dundas, C.M., Kirk, R.L., 2009.
692 Observations of periglacial landforms in Utopia Planitia with the High Resolution Imaging
693 Science Experiment (HiRISE) Journal of Geophysical Review 114, E04005, doi:10.1029/
694 2008JE003264.
695 Levy, J.S., Head, J., Marchant, D. 2009. Thermal contraction crack polygons on Mars:
696 Classification, distribution, and climate implications from HiRISE observations. Journal of
697 Geophysical Research 114, E01007, doi:10.1029/2008JE003273.
698 Lucchitta, B., 1981. Mars and Earth: Comparison of cold-climate features. Icarus 45, 264-303.
699 Mackay, J.R., 1972. The world of underground ice. Annals of the Association of American
700 Geographers 62, 1, 1-22.
701 Mackay, J.R., 1974. Ice wedge cracks, Garry Island, Northwest Territories, Canadian Journal of
702 Earth Science 11, 1366-1383.
703 Mackay, J.R., 1978. A full-scale field experiment (1978-1995) on the growth of permafrost by
704 means of lake drainage, western Arctic coast: a discussion of the method and some results.
705 Canadian Journal of Earth Sciences 34, 17-33.
706 Mackay, J.R., Matthews, J.V., 1983. Pleistocene ice and sand wedges, Hooper Island, Northwest
707 Territories. Canadian Journal of Earth Sciences 20, 1087-1098.
708 Mackay, J.R., 1998. Pingo growth and collapse, Tuktoyaktuk Peninsula areas, western arctic
709 coast, Canada: a long-term field study. Géographie physique et Quaternaire 52, 3, 1-53.
710 Mackay, J.R., 1999. Periglacial features developed on the exposed lake bottoms of seven

711 lakes that drained rapidly after 1950, Tuktoyaktuk Peninsula Area, western arctic coast,
712 Canada. Permafrost and Periglacial Processes. 10, 39-63.
713 Madeleine, J-B., Forget, F., Head, J.H., Levrard, B., Montmessin, F., Millour, E., 2009.
714 Amazonian northern mid-latitude glaciation on Mars: A proposed climate scenario Icarus
715 203, 390-405, doi:10.1016/j.icarus.2009.04.037.
716 Malin, M.C., et al., 2007. Context Camera investigation on board the Mars Reconnaissance
717 Orbiter. Journal of Geophysical Research 112, E05S04. doi:10.1029/ 20 06JE0 02808.
718 Marchant, D.R. et al., 2002. Formation of patterned ground and sublimation till over Miocene
719 glacier ice in Beacon Valley, southern Victoria Land, Antarctica. Geological Society of
720 America Bulletin 114, 6, 718-730.
721 McEwen, A.S., et al., 2007. Mars Reconnaissance Orbiter's High Resolution Imaging Science
722 Experiment (HiRISE). Journal of Geophysical Research 112, E05S02, doi:10.1029/2005/
723 JE002605.
724 Mellon, M.T., Jakosky, B.M., 1993. Geographic variations in the thermal and diffusive stability
725 of ground ice on Mars. Journal of Geophysical Research 98, E2, 3345-3364.
726 Michael, G.G., Neukum, G., 2010. Planetary surface dating from crater size-frequency distribution
727 measurements: partial resurfacing events and statistical age uncertainty. Earth and
728 Planetary Science Letters 294, 223-229, doi:10.1016/j.epsl.2009.12.041.
729 Milliken, R.E., Mustard J.F., Goldsby, D.L., 2003. Viscous flow features on the surface of Mars:
730 Observations from high-resolution Mars Orbiter Camera (MOC) images. Journal of
731 Geophysical Research 108, E6, 5057, doi:10.1029/2002JE002005.
732 Morgenstern, A., Hauber, E., Reiss, D., van Gasselt, S., Grosse, G., Schirrmeister, L., 2007.

733 Deposition and degradation of a volatile-rich layer in Utopia Planitia and implications for
734 climate history on Mars. Journal of Geophysical Research 112, E06010, doi:10.1029/2006
735 JE002869.
736 Morgenstern, A., Ulrich, M., Günther, F., Roessler, S., Fedorova, I.V., Rudaya, N.A., Wetterich,
737 S., Boike, J., Schirrmeister, L., 2013. Evolution of thermokarst in East Siberian ice-rich
738 permafrost: a case study. Geomorphology 201, 363-379, doi.org/10.1016/j.geomorph.
739 2013.07.011.
740 Müller, F., 1962. Analysis of some stratigraphic observations and radiocarbon dates from two
741 pingos in the Mackenzie Delta area, N.W.T. Arctic 15, 4, 279-288.
742 Murton, J.B., 1996. Thermokarst-lake basin sediments, Tuktoykatuk Coastlands, western arctic
743 Canada. Sedimentology 43, 737-760.
744 Murton, J.B., 2005. Ground-ice stratigraphy and formation at North Head, Tuktoyaktuk
745 Coastlands, Western Arctic Canada: a product of glacier-permafrost interactions.
746 Permafrost and Periglacial Processes 16, 31-50, doi:10.1002/ppp.513.
747 Murton, J.B., Worsley, P., Gozdsik, J., 2000. Sand veins and wedges in cold aeolian
748 environments. Quaternary Science Reviews 19, 899-922.
749 Mustard, J.F., Cooper, C.D., Rifkin, M.K., 2001. Evidence for recent climate change on Mars
750 from the identification of youthful near-surface ground ice. Nature 412, 411-414, doi:10.
751 1038/35086515.
752 Ohja, L., Wilhelm, M.B., Murchie, S.L., McEwen, A.S., Wray, J.J., Hanley, J., Massé, M.,
753 Chojnacki, M., 2015. Spectral evidence for hydrated salts in recurring slope lineae on Mars.
754 Nature Geoscience 8, 829-832, doi.org/10.1038/ngeo2546.
755 Osinski, G.R., Soare, R.J., 2007. Circular structures in Utopia Planitia, Mars: impact vs periglacial

origin and implications for assessing ground ice content. 38th Lunar and Planetary Science Conference, Houston, Texas. Abstract # 1609.

Parker, T.J., Gorsline, D.S., Saunders, R.S., Pieri, D.S., Schneeberger, D.M., 1993. Coastal geomorphology of the Martian northern plains. Journal of Geophysical Research 98, E6, 11,061-11,078.

Penner, E., 1959. The mechanism of frost heaving in soils. Highway Research Board Bulletin 225, 1-22.

Péwé, T.L., 1954. Effect of permafrost on cultivated fields, Fairbanks area, Alaska. U.S. Geological Survey Bulletin 989-F, 315-351.

Péwé, T.L., 1959. Sand-wedge polygons (tessellations) in the McMurdo Sound region, Antarctica-a progress report. American Journal of Science 257, 545-552.

Porsild, A.E., 1938. Earth mounds in unglaciated arctic northwestern America. Geographical Review, 28, 1, 46-58.

Primm, K.M., Gough, R.V., Chevrier, V.F., Tolbert, M.A., 2017. Freezing of perchlorate and chloride brines under Mars-relevant conditions. Geochimica et Cosmochimica Acta 212, 211-220, dx.doi.org/10.1016/j.gca.2017.06.012.

Rampton, V.N., 1988. Quaternary geology of the Tuktoyaktuk Coastlands, Northwest Territories, Geological Society of Canada, Memoir 423, 98 p.

Rampton, V.N., Mackay, J.R., 1971. Massive ice and icy sediments throughout the Tuktoyaktuk Peninsula, Richards Island, and nearby areas, District of Mackenzie, Geological Survey of Canada, Paper 71-21, 16 p.

Rampton, V.N., Bouchard, M., 1974. Surficial geology of Tuktoyaktuk, District of Mackenzie. Geological Survey of Canada, Paper 74-53, 17 p.

779 Rossbacher, L.R., Judson, S., 1981. Ground ice on Mars: inventory, distribution and resulting
780 landforms. Icarus 45, 35-59.
781 Samsonov, S.V., Lantz, T.C., Kokelj, S.V., Zhang, Y., 2016. Growth of a young pingo in the
782 Canadian arctic observed by RADARSAT-2 interferometric satellite radar. Cryosphere 10,
783 799-810, doi:10.5194/tc-10-799-2016.
784 Schirrmeister, L., Siegert, C., Kunitzky, V.V., Grootes, P.M., Erlenkeuser, H., 2002. Late
785 Quaternary ice-rich permafrost sequences as a paleoenvironmental archive for the Laptev
786 Sea Region is northern Siberia. International Journal of Earth Sciences 91, 154-167,
787 doi:10.1007/s005310100205.
788 Schirrmeister, L., Froese, D., Tumskoy, V., Grosse, G. & Wetterich, S., 2013. Yedoma: late
789 Pleistocene ice-rich syngenetic permafrost of Beringia. In: Elias, S.A., (ed.) The
790 Encyclopedia of Quaternary Science 3, 542-552. Amsterdam: Elsevier.
791 Schirrmeister, L., Bobrov, A., Raschke, E., Herzschuh, U., Strauss, J., Pestryakova, L.A.,
792 Wetterich, S., 2018. Late Holocene ice-wedge polygon dynamics in northeastern Siberian
793 coastal lowlands. Arctic, Antarctic, and Alpine Research, 50, 1, e1462595, doi:10.1080/
794 15230430.2018.1462595.
795 Schorghofer, N., 2007. Dynamics of ice ages on Mars. Nature 192-195, 449, doi:10.1038/nature
796 06082.
797 Seibert, N.M., Kargel, J.S., 2001. Small scale Martian polygonal terrain: implications for liquid
798 surface water. Geophysical Research Letters 28, 5, 899-902.
799 Séjourné, A. Costard, F.N., Gargani, J., Soare, R.J., Marmo, C., 2010. The polygon junction pits
800 as evidence of a particularly ice-rich area of Utopia Planitia. 41st Lunar and Planetary
801 Science Conference, Houston, Texas. Abstract # 2113.

802 Séjourné, A. Costard, F.N., Gargani, J., Soare, R.J., Federov, A., Marmo, C., 2011. Scalloped
803 terrain and small-sized polygons in western Utopia Planitia, Mars: a new formation
804 hypothesis. Planetary and Space Science 59, 412-422, doi:10.1016/j.pss.2011.01.007.
805 Sharp, R.P., Soderblom, L.A., Murray, B.C., Cutts, J.A., 1971. The surface of Mars, uncratered
806 terrain. Journal of Geophysical Research 76, 2, 331-342.
807 Sharp, R.P., 1973. Mars: fretted and chaotic terrains. Journal of Geophysical Review 78, 20, 4073-
808 4083.
809 Sizemore, H. G., Zent, A.P., Rempel, A.W., 2015. Initiation and growth of Martian ice lenses.
810 Icarus 251, 191–210, doi.org/10.1016/j.icarus.2014.04.013.
811 Sletten, R.S., Hallet, B., Fletcher, R.C., 2003. Resurfacing time of terrestrial surfaces by the
812 formation and maturation of polygonal patterned ground. Journal of Geophysical Research
813 108, E4, 8044, dx.doi.org/10.1029/2002JE001914.
814 Smith, M.R., Gillespie, A.R., Montgomery, D.R., 2008. Effect of obliteration on crater count
815 chronologies for Martian surfaces. Geophysical Research Letters 35, L10202,
816 doi:10.1029/2008GL033538.
817 Soare, R.J., Burr, D.M., Wan Bun Tseung, J-M., 2005. Pingos and a possible periglacial landscape
818 in northwest Utopia Planitia, Mars. Icarus 174, 373-382, doi.org/10.1016/j. icarus.2004.11.
819 013.
820 Soare, R.J., Osinski, G.R., Roehm, C.L., 2008. Thermokarst lakes and ponds on Mars in the very
821 recent (late Amazonian) past. Earth and Planetary Science Letters 1-2, 382-393, doi.org/
822 10.1016/j.epsl.2008.05.010.
823 Soare, R.J., Osinski, G.R. 2009. Stratigraphical evidence of late Amazonian periglaciation and

824 glaciation in the Astapus Colles region of Mars. Icarus 202, 17-21, doi:10.1016/j.icarus.
825 2009.02.009.
826 Soare, R.J., Séjourné, A., Pearce, G., Costard, F., Osinski, G.R., 2011. The Tuktoyaktuk coastlands
827 of northern Canada: a possible "wet" periglacial analogue of Utopia Planitia, Mars.
828 Geological Society of America 483, 203-218, doi.org/10.1130/2011.2483(13).
829 Soare, R.J., Conway, S.J., Pearce, G.D., Costard, F., Séjourné, A., 2013a. Sub-kilometre (intra-
830 crater) mounds in Utopia Planitia, Mars: character, occurrence and possible formation
831 hypotheses. Icarus 225, 982-991, dx.doi.org/10.1016/j.icarus.2012.06.003.
832 Soare, R.J., Conway, S.J, Pearce, G., Dohm, J.M., Grindrod, P.M., 2013. Possible crater-based
833 pingos, paleolakes and periglacial landscapes in the high latitudes of Utopia Planitia, Mars.
834 Icarus, 225, 2, 971-981, doi.org/10.1016/j.icarus.2012.08.041.
835 Soare, R.J., Conway, S.J., Dohm, J.M., 2014a. Possible ice-wedge polygons and recent landscape
836 modification by "wet" periglacial processes in and around the Argyre impact basin, Mars
837 Icarus 225, 2, 971-981, doi.org/10.1016/j.icarus.2012.08.041.
838 Soare, R.J., Conway, S.J., Dohm, J.M., El-Maarry, M.R., 2014b. Possible open-system pingos in
839 and around the Argyre impact basin, Mars. Earth and Planetary Science Letters 398, 25-
840 36, doi.10.1016/j.epsl.2014.04.044.
841 Soare, R.J., Horgan, B., Conway, S.J., Souness, C., El-Maarry, M.R., 2015. Volcanic terrain and
842 the possible periglacial formation of "excess ice" at the mid-latitudes of Utopia Planitia,
843 Mars. Earth and Planetary Science Letters 423, 182-192, dx.doi.org/10.1016/j.epsl.2015.
844 04.033.
845 Soare, R.J., Conway, S.J., Gallagher, C., Dohm, J.M., 2017. Ice-rich (periglacial) vs icy (glacial)

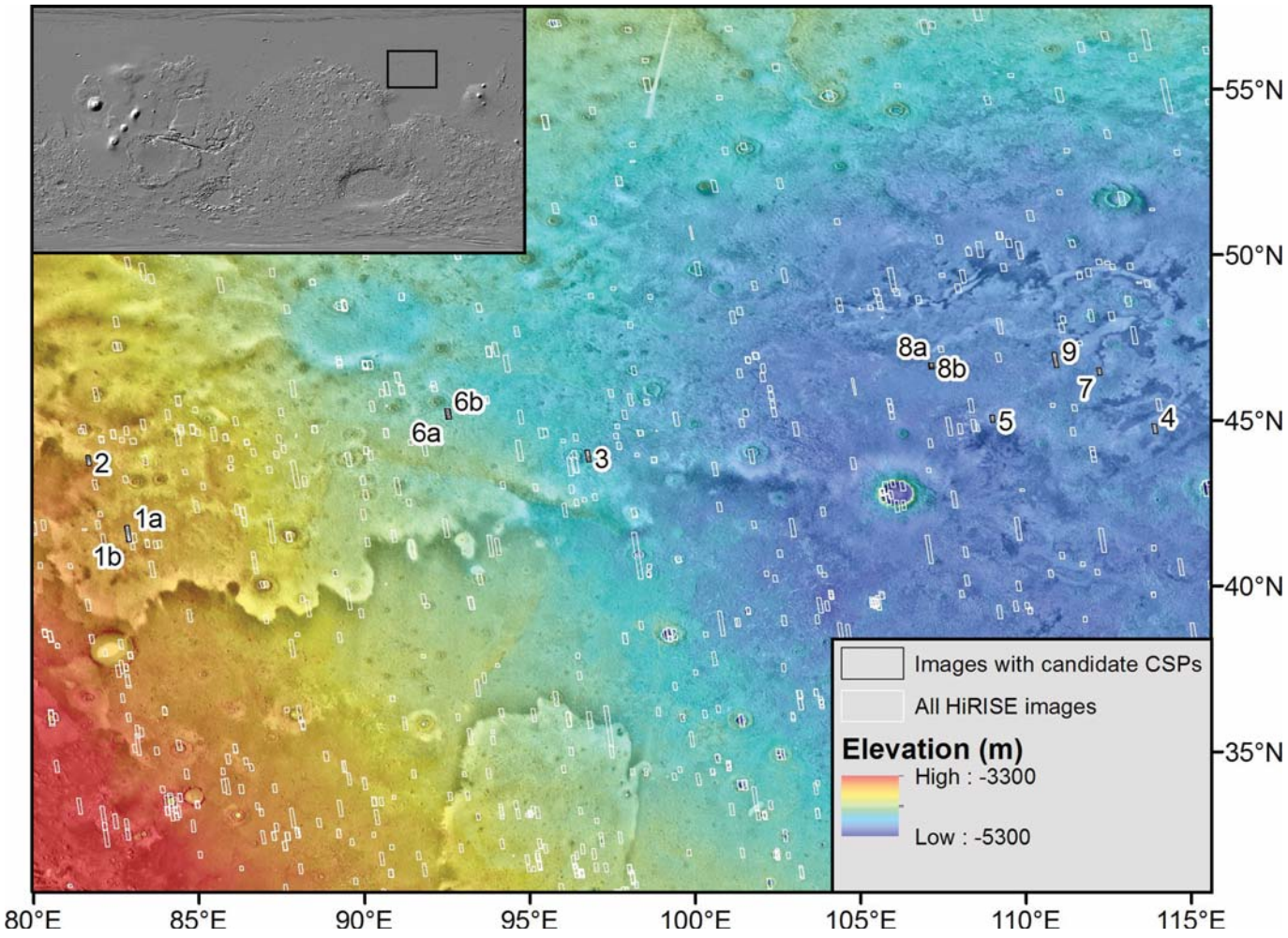
55°N
50°N
45°N
40°N
35°N
80°E
85°E
90°E
95°E
100°E
105°E
110°E
115°E
1a
1b
2
3
4
5
6a
6b
7
8a
8b
9
Images with candidate CSPs
All HiRISE images
Elevation (m)
High : -3300
Low : -5300

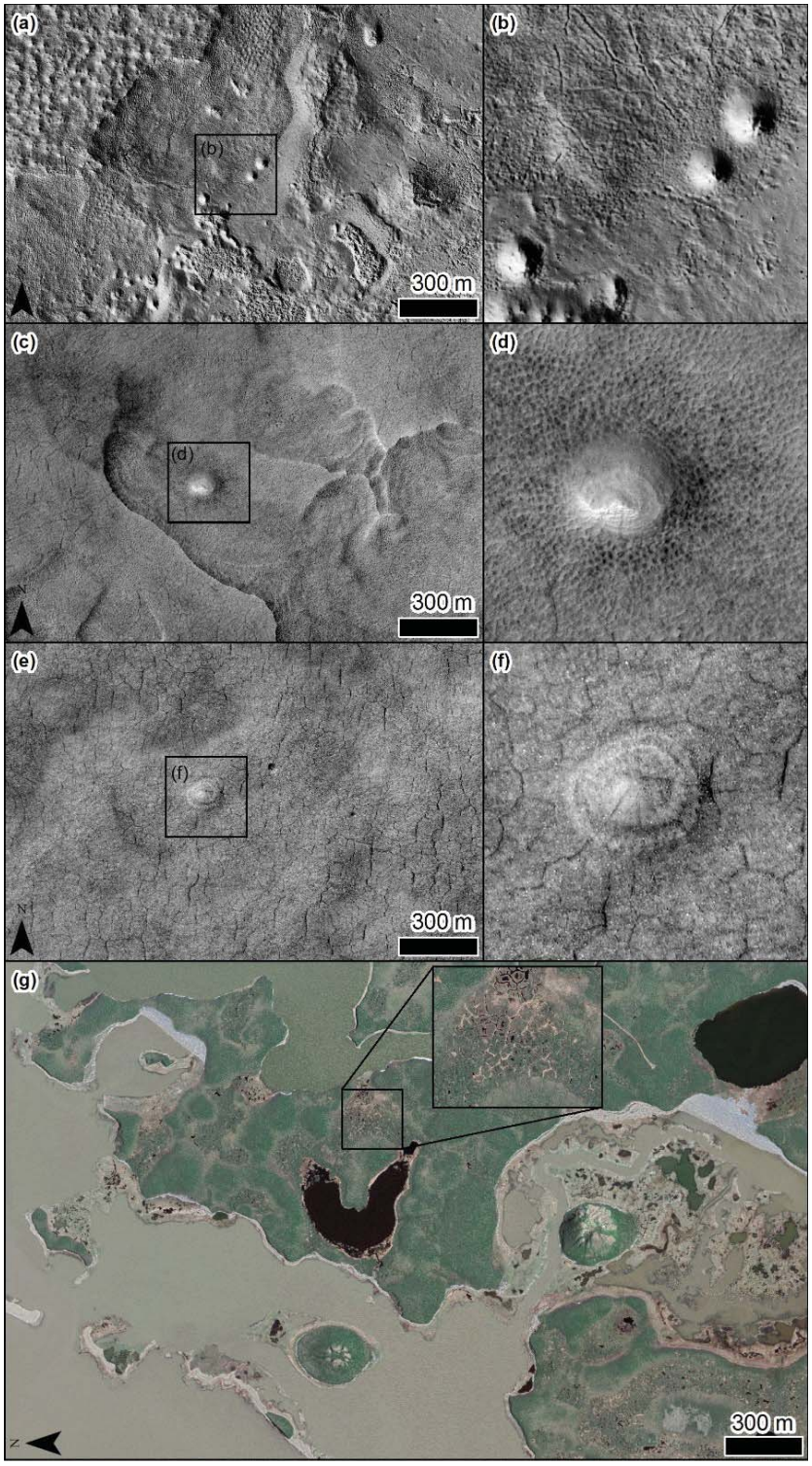
(a)
(b)
300 m
(b)
(c)
(d)
300 m
(d)
(e)
(f)
300 m
(f)
(g)
300 m

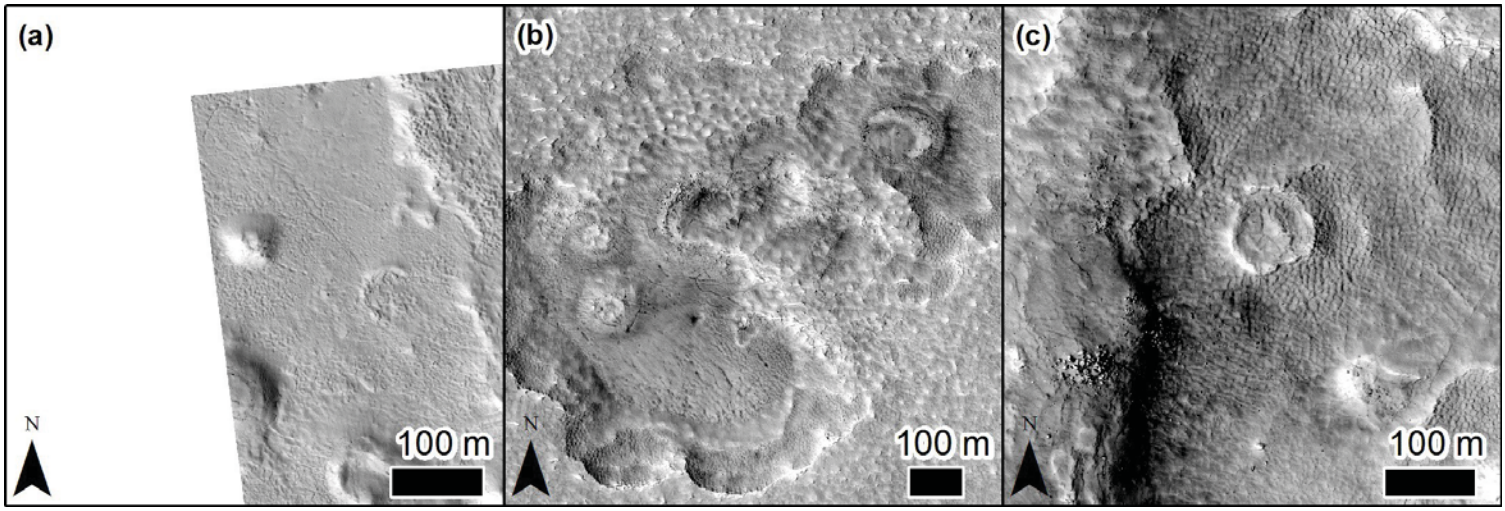
(a)
N
100 m
(b)
N
100 m
(c)
N
100 m

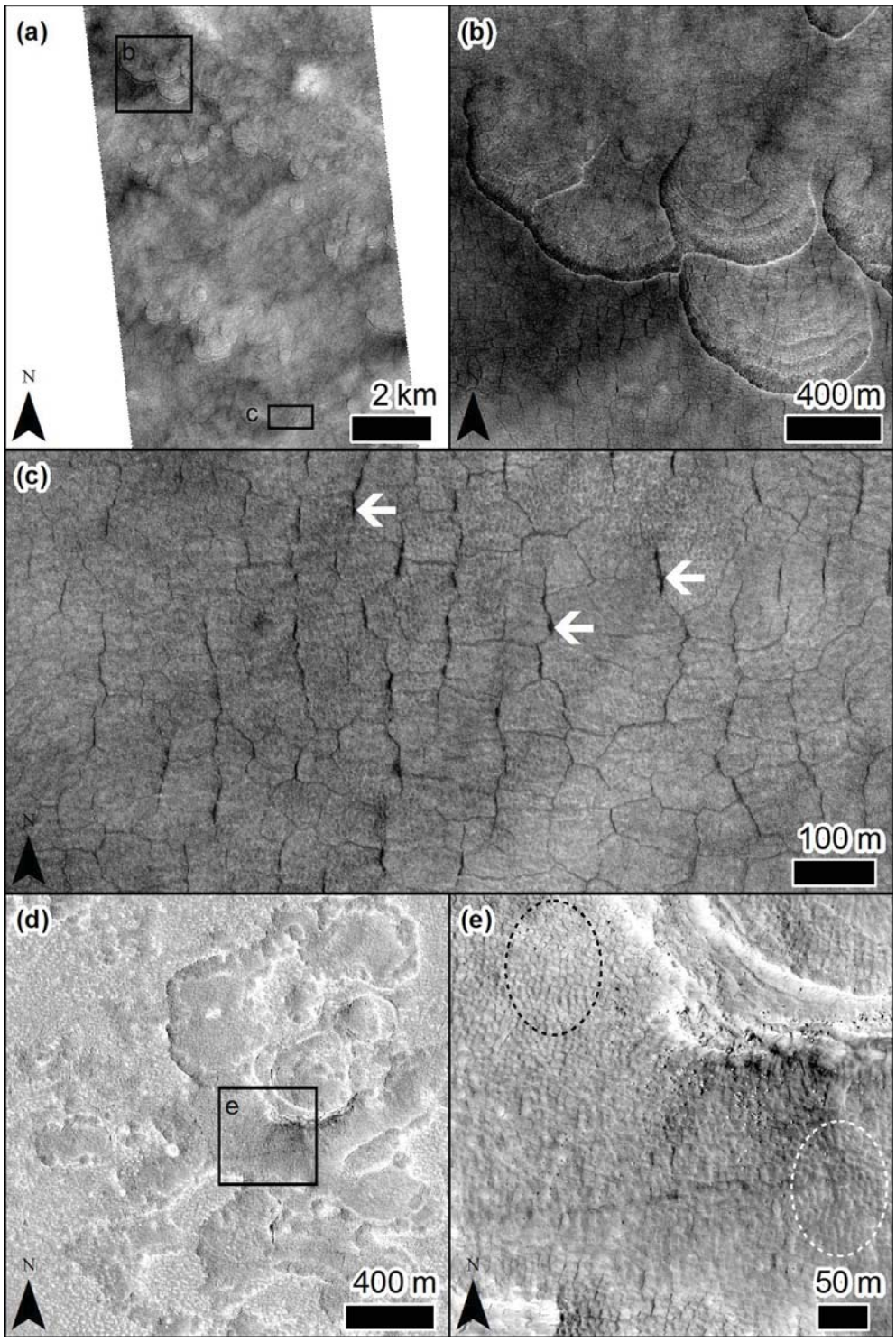
(a)
b
c
N
2 km
(b)
400 m
(c)
N
100 m
(d)
e
N
400 m
(e)
N
50 m

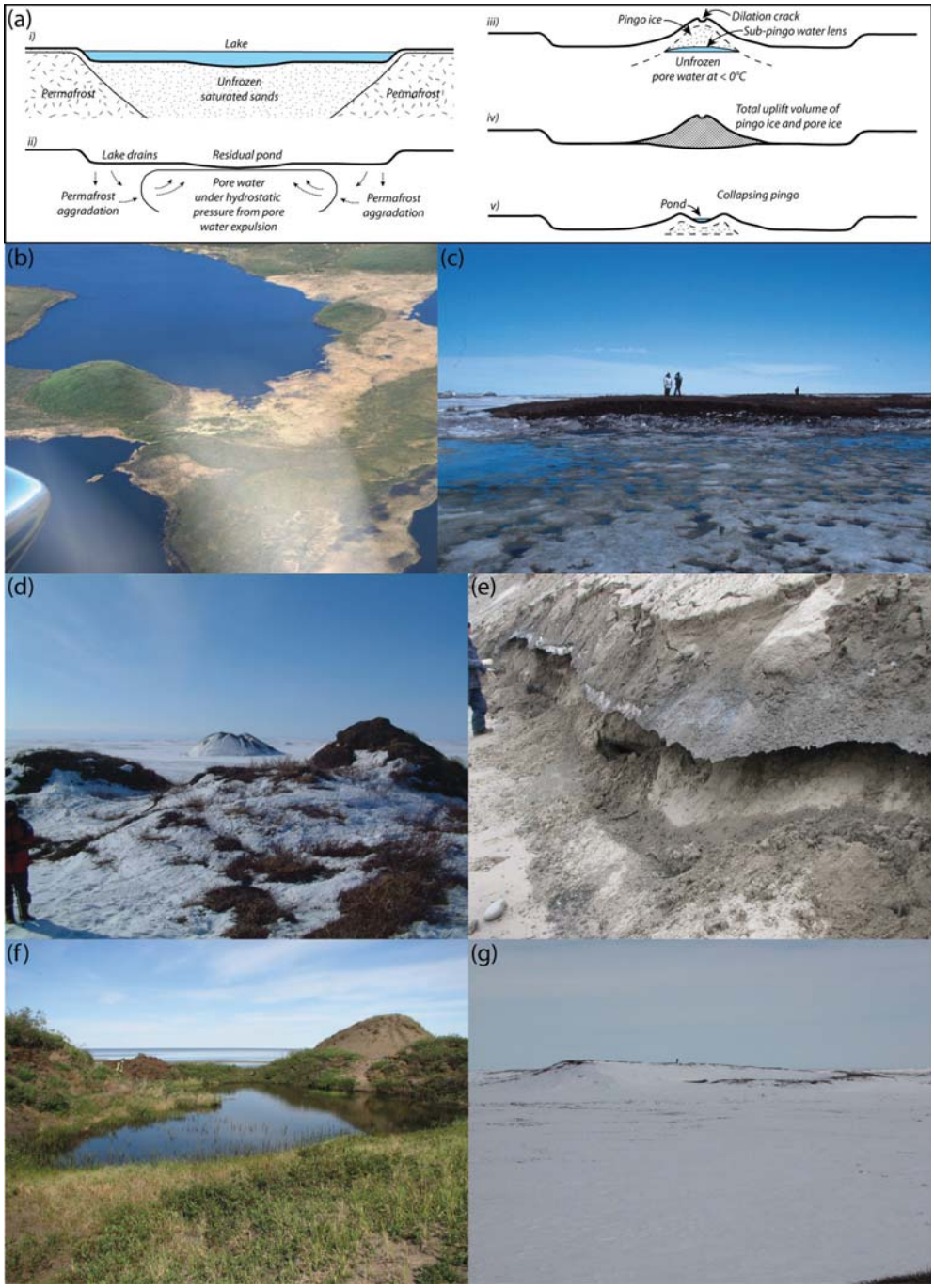
(a)
i)
Lake
Permafrost
Unfrozen
saturated sands
Permafrost
ii)
Lake drains
Residual pond
Permafrost
aggradation
Pore water
under hydrostatic
pressure from pore
water expulsion
Permafrost
aggradation
iii)
Pingo ice
Dilation crack
Sub-pingo water lens
Unfrozen
pore water at < 0°C
iv)
Total uplift volume of
pingo ice and pore ice
v)
Pond
Collapsing pingo
(b)
(c)
(d)
(e)
(f)
(g)

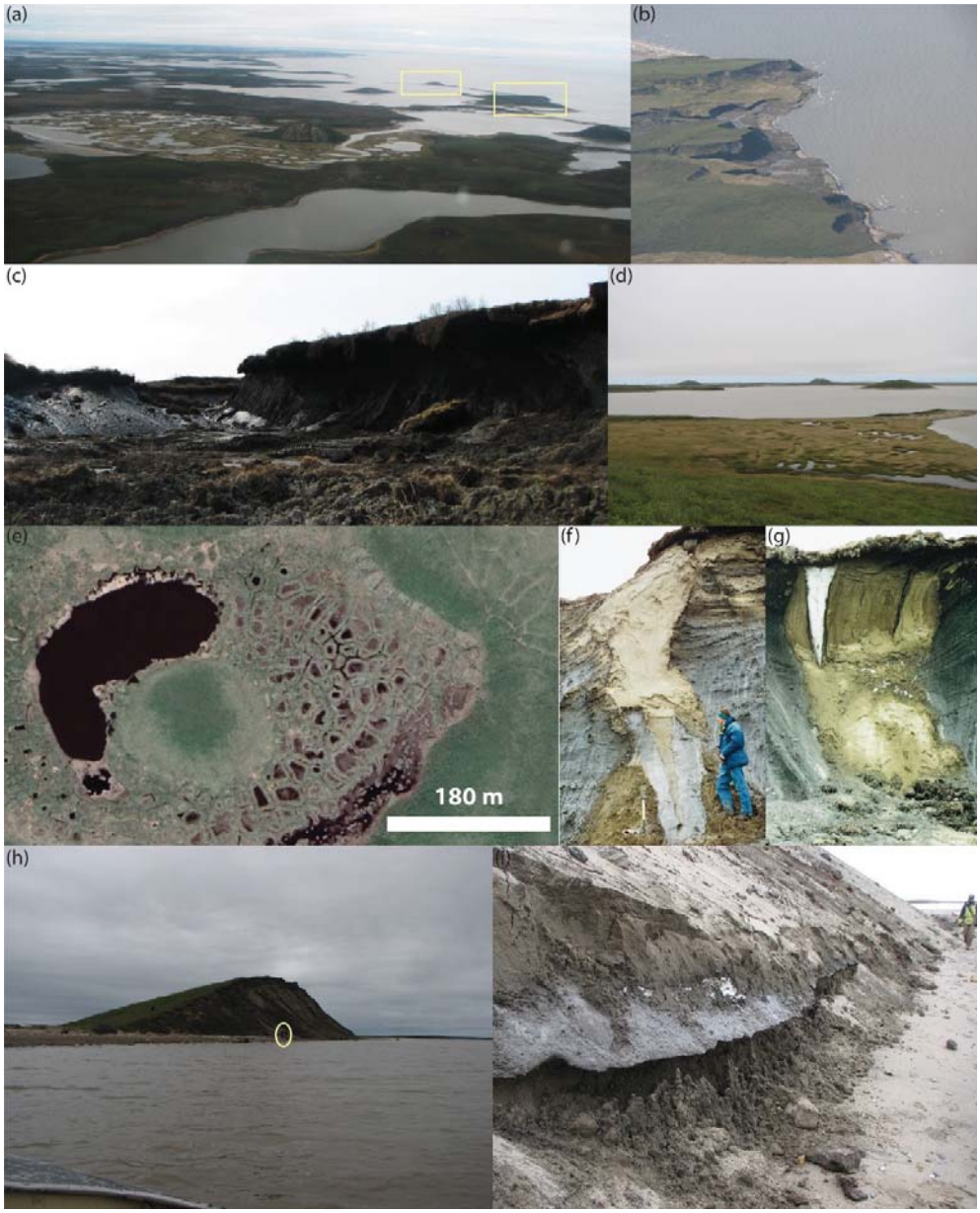
(a)
(b)
(c)
(d)
(e)
180 m
(f)
(g)
(h)
(i)

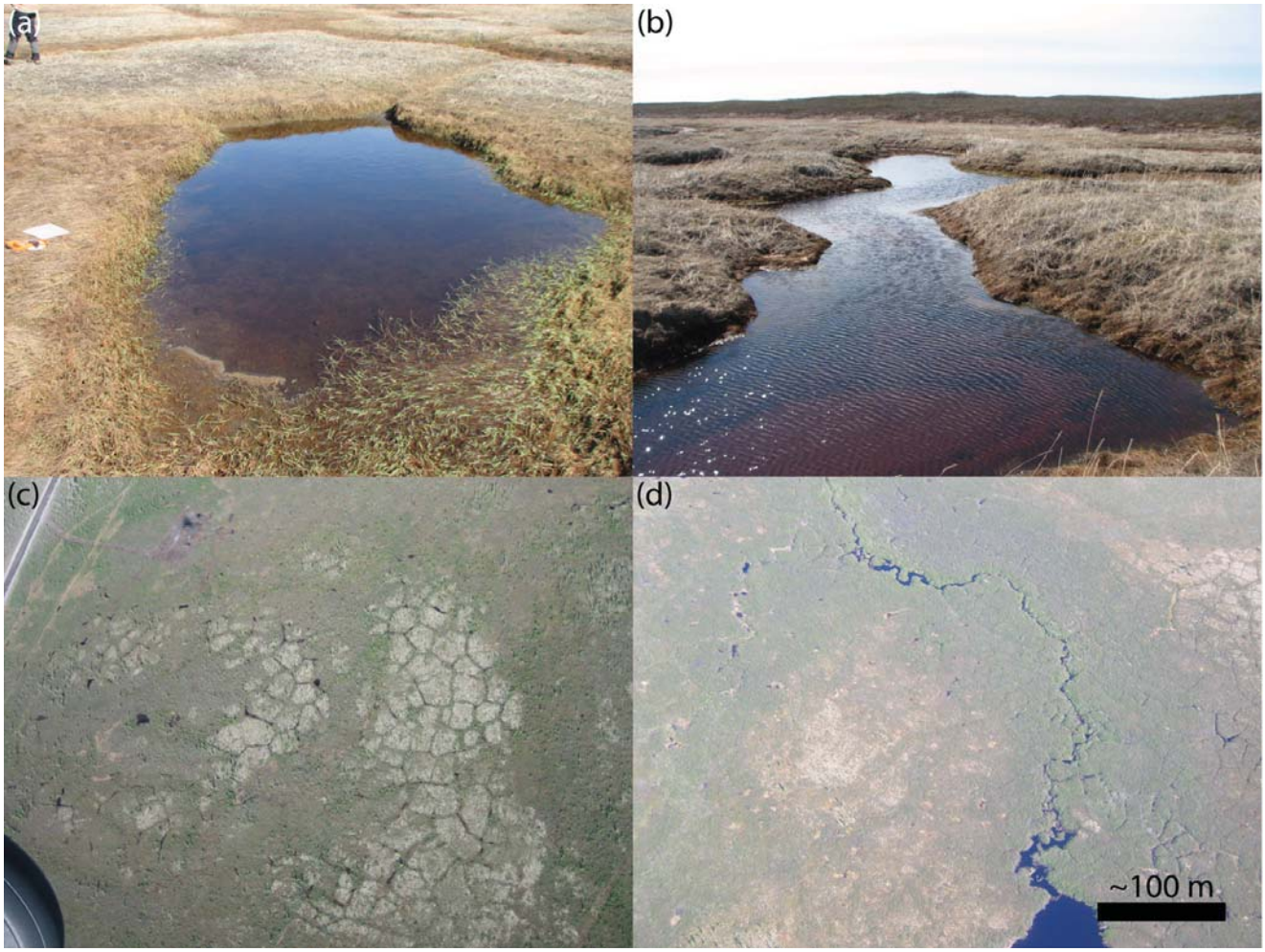
(a)
(b)
(c)
(d)
~100 m

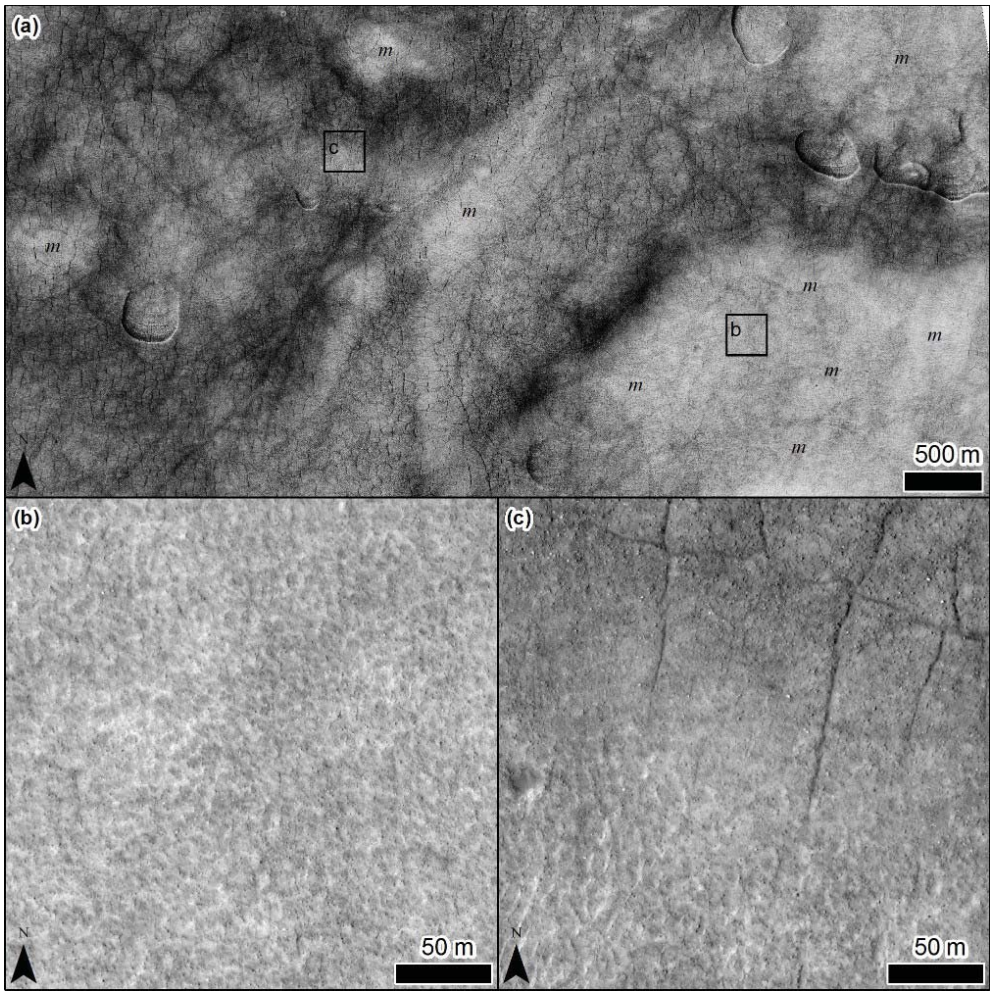
(a)
m
m
c
m
m
m
b
m
m
m
m
N
500 m
(b)
N
50 m
(c)
N
50 m

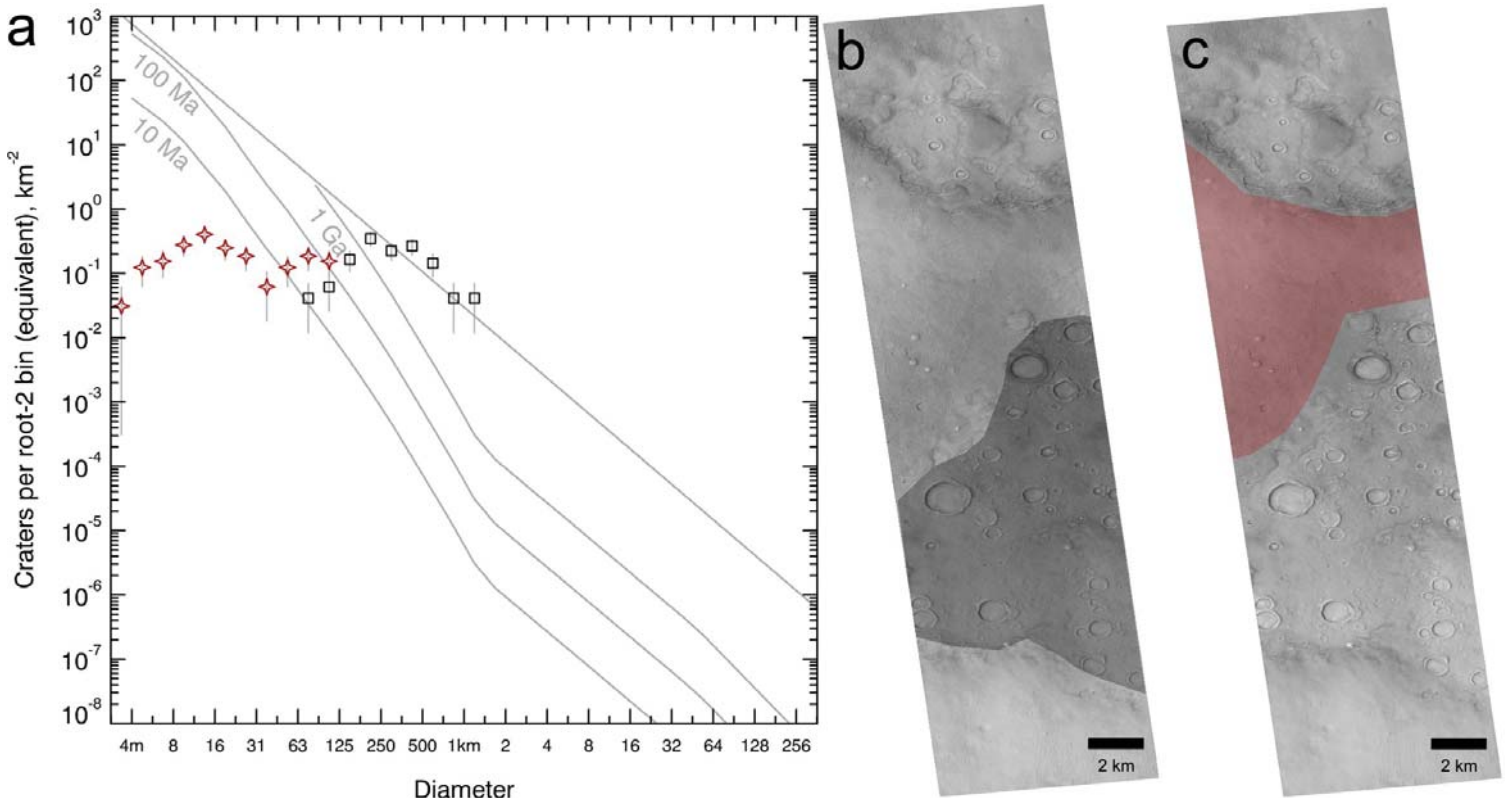
a
b
c
100 Ma
10 Ma
1 Ga
Craters per root-2 bin (equivalent), km-2
Diameter
4m
8
16
31
63
125
250
500
1km
2
4
8
16
32
64
128
256
2 km
2 km

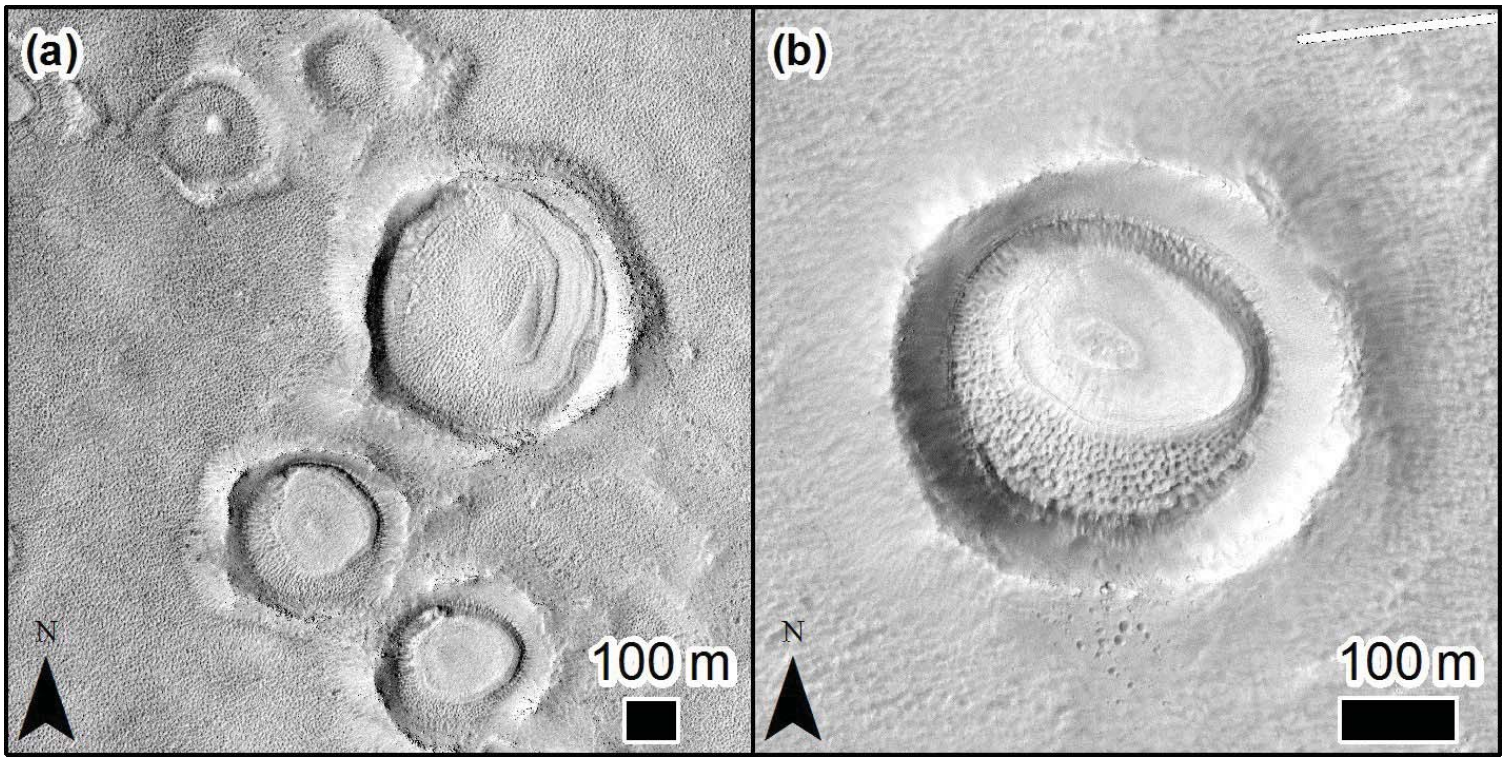
(a)
N
100 m
(b)
N
100 m

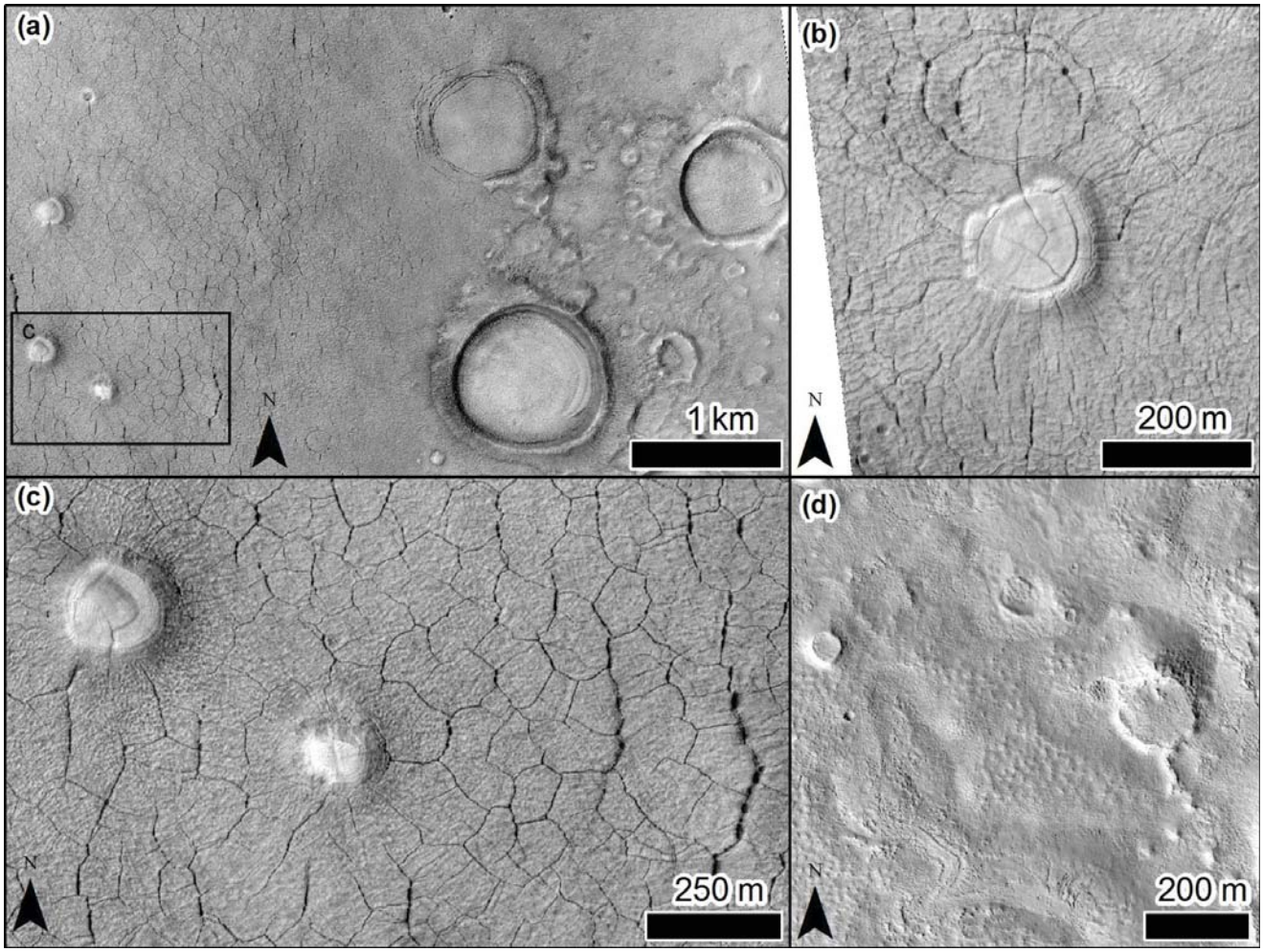
(a)
c
N
1 km
(b)
N
200 m
(c)
N
250 m
(d)
N
200 m

Table 1: Candidate closed-system pingos, *CSPs*, in the zone 35-50°N; 80-115°E from 453 *HiRISE* images.

Candidate *CSP* locations	HiRISE Image ID	Resolution (pixel/cm)	Centre Latitude	Centre Longitude	Candidate *CSPs* (#)	Summit-fracturing [f], -depression [d],-tiered [t] or irregular topography [it]	Candidate *CSPs* (# collapsed)	Scalloped-depression distribution (complexes [c];	Polygonised terrain	High-centred polygons	Low-centred polygons	Polygon-junction and margin pits
1a	PSP_008162_2220	25	41.583	82.850	1	it	-	c	x	?	?	x
1b	PSP_007951_2220	25	41.587	82.849	1	it	-	c	x	?	?	x
2	ESP_044042_2240	25	43.796	81.653	1	it	-	c	x	?	?	x
3	ESP_026556_2245	50	43.930	96.746	2	f,d,t	-	c	x	?	?	x
4	ESP_055038_2250	50	44.757	113.888	61	d, t, it	1	c	x	x	x	-
5	ESP_026727_2255	25	45.052	108.977	3	t, it	1	c	x	x	x	-
6a	PSP_008913_2255	25	45.206	92.528	1	t	-	c	x	?	?	x
6b	PSP_008979_2255	25	45.206	92.529	1	t	-	c	x	?	?	x
7	ESP_027650_2275	50	46.479	112.218	7	2	5	c	x	x	x	-
8a	ESP_053535_2270	25	46.671	107.139	2	it	-	c	x	x	x	-
8b	PSP_009163_2270	25	46.651	107.138	2	it	-	c	x	x	x	-
9	ESP_026450_2270	50	46.823	110.880	2	it	1	c	x	x	x	-